Comparison and evaluation of methods to infer gene regulatory networks from multimodal single-cell data

Pau Badia-i-Mompel[1,2], Roger Casals-Franch[1,3,4], Lorna Wessels[1], Sophia Müller-Dott[1], Rémi Trimbour[5], Yunxiao Yang[6], Ricardo O. Ramirez Flores[7,#], Julio Saez-Rodriguez[1,7,#,*]

[1] Heidelberg University, Faculty of Medicine, and Heidelberg University Hospital, Institute for Computational Biomedicine, Heidelberg, Germany

[2] GSK, Cellzome, Heidelberg, Germany

[3] Institut de Recerca i Innovació en Ciències de la Vida i de la Salut a la Catalunya Central (IRIS-CC), Vic, Catalonia, Spain.

[4] Department of Biosciences, Faculty of Sciences and Technology, Universitat de Vic—Universitat Central de Catalunya, Vic, Spain

[5] Institut Pasteur, Université Paris Cité, CNRS UMR 3738, Machine Learning for Integrative Genomics Group, Paris, France

[6] Department of Biomedical Engineering and McKusick-Nathans Department of Genetic Medicine, Johns Hopkins University, Baltimore MD, USA

[7] European Molecular Biology Laboratory, European Bioinformatics Institute (EMBL-EBI), Hinxton, Cambridgeshire, U.K.

[#] These two authors jointly supervised this work

* Corresponding author: saezlab@ebi.ac.uk

Abstract

Cells regulate their functions through gene expression, driven by a complex interplay of transcription factors and other regulatory mechanisms that together can be modeled as gene regulatory networks (GRNs). The emergence of single-cell multi-omics technologies has driven the development of several methods that integrate transcriptomics and chromatin accessibility data to infer GRNs. While these methods provide examples of their utility in discovering new regulatory interactions, a comprehensive benchmark evaluating their mechanistic and predictive properties as well as their ability to recover known interactions is lacking. To address this, we built a comprehensive framework, Gene Regulatory nETwork Analysis (GRETA), available as a Snakemake pipeline, that includes state of the art methods decomposing their different steps in a modular manner. With it, we found that the GRNs were highly sensitive to methods' choices, such as changes in random seeds, or replacing steps in the inference pipelines, as well as whether they use paired or unpaired multimodal data. Although the obtained networks performed moderately well in predictive evaluation tasks and partially recovered known interactions, they struggled to capture causal relationships from perturbation assays. Our work brings attention to the challenges of inferring GRNs from single-cell omics, offers guidelines, and presents a flexible framework for developing and testing new approaches.

Keywords: gene regulatory network, gene regulation, methods, benchmark, multi-omic, single cell

Graphical Abstract

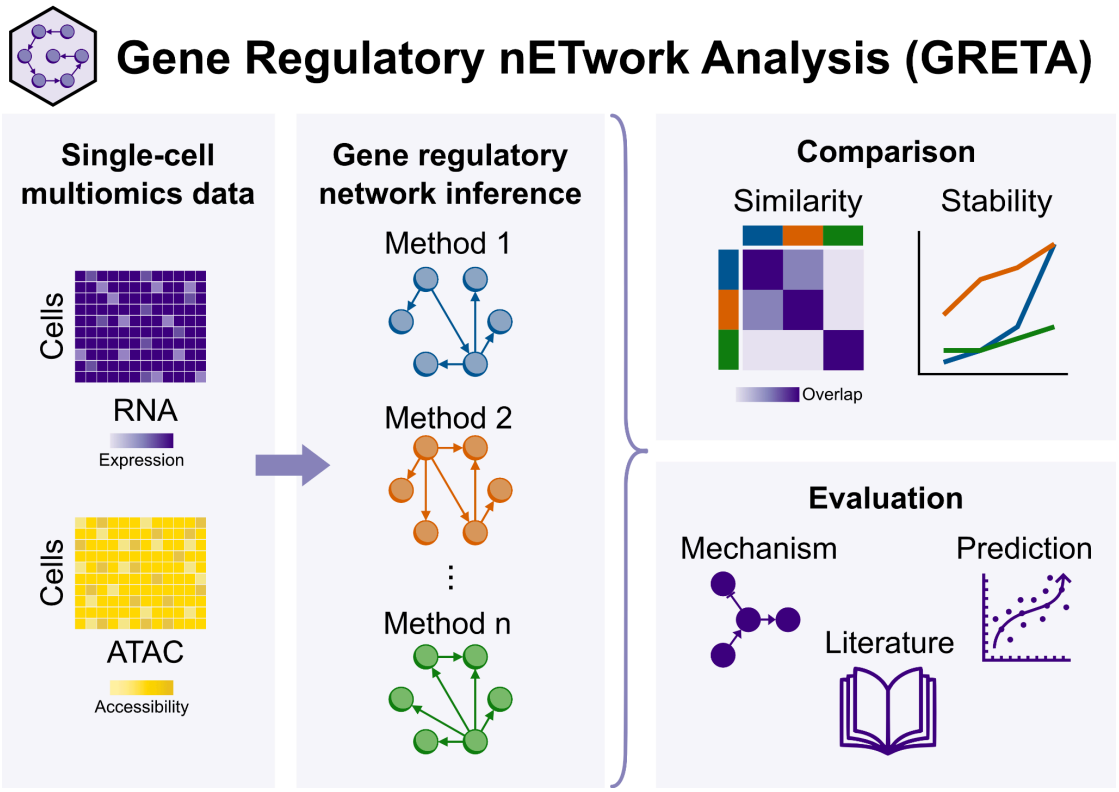

1. Introduction

Cells regulate transcription in response to intracellular and extracellular signals, primarily through transcription factors (TFs), a family of proteins that bind DNA to influence gene expression[1]. Genomic DNA is tightly packed into chromatin, rendering most genes inaccessible. Pioneer TFs can initiate changes in DNA accessibility, while other TFs bind to proximal regions like promoters or distal cis-regulatory elements (CREs) to recruit and stabilize the RNA polymerase complex for mRNA synthesis from the gene body[1]. Alternatively, TFs can also reduce gene accessibility, impeding the transcription machinery and suppressing gene expression[1].

The interactions between DNA regions, TFs, target genes and other molecules form intricate regulatory circuits, which can be modeled as gene regulatory networks (GRNs)[2–4]. These networks are typically represented as graphs, where nodes represent TFs and genes, and edges indicate regulatory relationships between them. These interactions can be positive, where a TF activates expression of a gene, or negative, where it inhibits it. The group of target genes regulated by a TF is known as a TF regulon, and the collection of regulons form a GRN. The analysis of GRNs provides valuable insights into the processes by which cellular identity is established, maintained, and altered in disease[5,6].

Historically, GRNs have been inferred de-novo from experimental data[4], particularly bulk omics data, as well as from literature sources[7–9], which compile findings from multiple assays. The emergence of single-cell multi-omics technologies[10], particularly the joint profiling of single-cell transcriptomics (snRNA-seq) and chromatin accessibility (Assay for Transposase-Accessible Chromatin using sequencing; snATAC-seq), has driven the creation of advanced computational methods that integrate these multimodal data types. Although they use a variety of strategies, these methods perform the same four inference steps when linking TFs to target genes: processing of candidate TFs, CREs and genes; assigning CREs to neighbouring genes; predicting TF binding on CREs; and identifying the final TF-gene interactions through mathematical modelling.

Contrary to literature-derived GRNs, these methods potentially enable the inference of highly context-specific regulatory interactions. TF-gene interactions can vary depending on the chromatin state, making these approaches particularly promising for improving GRN reconstruction[11]. This is especially relevant given that transcriptomics-only methods have shown significant limitations in past benchmarks[12,13].

The joint modeling of these data types also comes with its own challenges, as current profiling technologies tend to yield sparse and noisy readouts, they require computational integration approaches, and have an increased computational cost due to the larger number of features considered[11]. Although multimodal GRN inference involves a sequence of shared steps across methods, their original implementations tend to be rigid, not allowing the use of other approaches in their pipeline. As a result, their application and comparison remain difficult tasks. Additionally, without technologies to directly measure interactions between regulatory elements and their effects on gene expression at large-scale, evaluating the resulting networks remains challenging[11–13]. A comprehensive benchmark of the existing methods is lacking, and it is thus still unclear how well these different methods perform, or even to which extent this joint modeling improves inference compared to methods that only use transcriptomics.

Here, we systematically compared five recently published multimodal single-cell GRN methods[14–18] alongside four alternative methods[8,9,19]. We first assessed the stability and overlap between methods, followed by an analysis of how paired versus unpaired multiomics data affect their results. Next, we examined the influence of different inference step combinations on GRN inference by decoupling the original steps of each multimodal method and testing all possible method-step combinations. Lastly, we developed a comprehensive set of mechanistic, predictive, and knowledge-based metrics to evaluate the original and decoupled versions of the methods. All results were generated using Gene Regulatory nETwork Analysis (GRETA, https://github.com/saezlab/greta), a free open-source framework to compare and evaluate multimodal GRN methods, implemented in a modular Snakemake[20] pipeline that allows to easily run any

combination of them. We found a high heterogeneity in the inferred GRNs, that is highly dependen on the choice of inference steps, and modest performance in benchmarks. Overall, our work underscores the complexity of GRN inference, offers guidelines to apply existing methods, and provides a flexible framework for the field to develop and benchmark new approaches.

2. Results

2.1. GRETA: A framework to systematically build, compare and evaluate gene regulatory networks from single-cell RNA and ATAC data

Multimodal methods that infer gene regulatory networks (GRNs) from single-nuclei transcriptomics (snRNA-seq) and chromatin accessibility (Assay for Transposase-Accessible Chromatin using sequencing, snATAC-seq) employ various strategies, that can be summarized into four main steps: (1) preprocessing data to identify candidate transcription factors (TFs), cis-regulatory elements (CREs), and genes; (2) linking CREs to neighboring genes based on genomic proximity to the transcription starting sites (TSSs) of genes, creating CRE-Gene edges; (3) predicting TF binding to CREs based on motif sequence similarity, forming TF-CRE-Gene triples; and (4) mathematical modeling to derive simplified TF-Gene interactions[11]. To evaluate the agreement between distinct GRN reconstruction methods from multimodal snRNA-seq and snATAC-seq data and to assess the impact of individual inference steps, we built Gene Regulatory nETwork Analysis (GRETA, https://github.com/saezlab/greta), a free and open-source modular Snakemake pipeline that decouples GRN inference steps, comparing and evaluating them (**Fig. 1**).

From paired or unpaired multimodal single-cell RNA-seq and ATAC-seq data, GRETA systematically executes the original implementation of five state-of-the-art multimodal methods[11] (*CellOracle*[14], *Dictys*[15], *FigR*[16], *GRaNIE*[17], and *Pando*[18]). It also provides their separate inference steps, enabling combinations to generate novel inference approaches. In addition, GRETA executes unimodal methods: *SCENIC*[19], the state-of-the-art GRN inference method for single-cell transcriptomics; two

prior knowledge based GRNs, *CollecTRI*[9] and *DoRothEA*[8]; and generates random networks with topological properties similar to the ones of inferred GRNs (**Methods**).

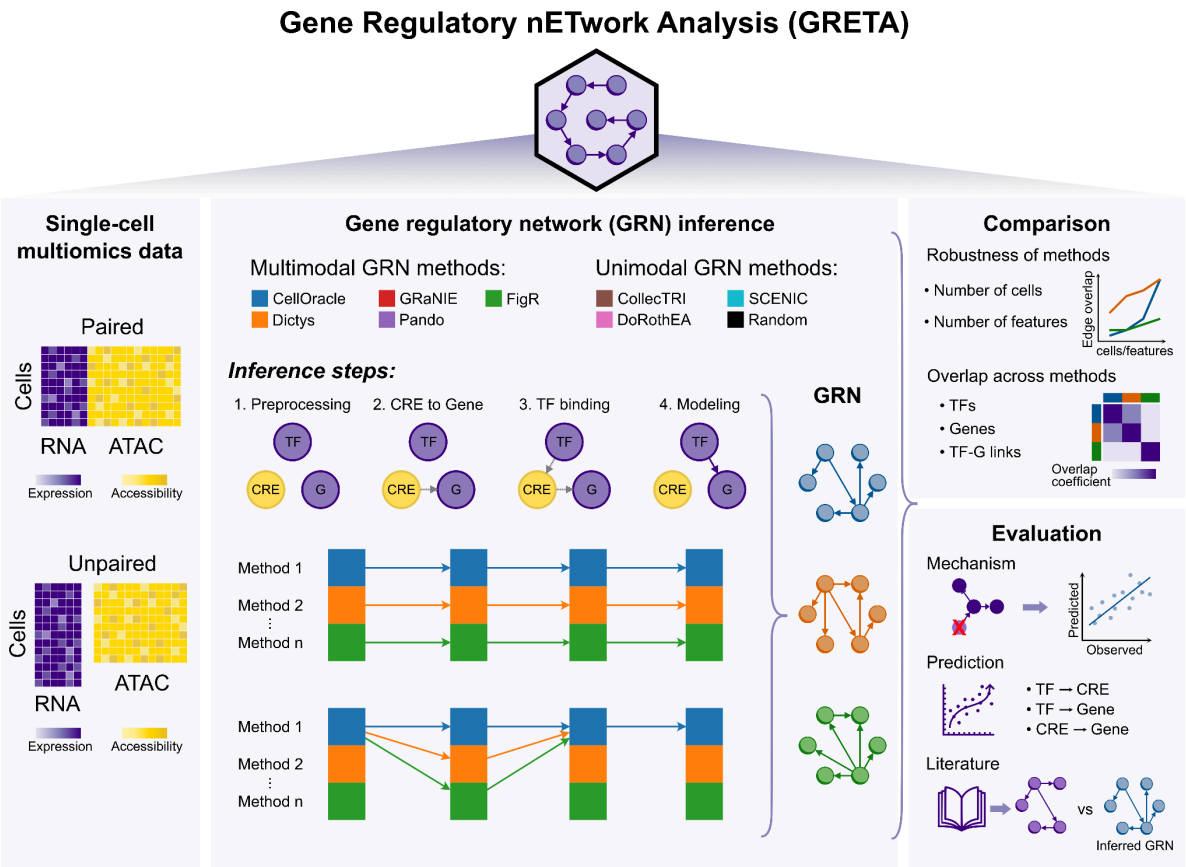

Figure 1. Gene Regulatory nETwork Analysis (GRETA). *GRETA is a flexible Snakemake pipeline designed to infer, compare, and evaluate gene regulatory networks (GRNs) from single-cell multimodal RNA-seq and ATAC-seq data. Its modular design allows for any combination of inference steps. GRNs generated with GRETA can be compared across TFs, edges, and target genes to assess stability under different conditions. Additionally, GRETA includes a collection of evaluation metrics categorized into three groups: mechanistic, predictive, and literature-based metrics.*

GRETA enables systematic comparison of GRNs at the TF, edge, and target gene levels. To account for differences in network sizes, it uses the overlap coefficient, defined as the intersection size between two sets divided by the smaller set's size. Using this statistic, it can also measure the robustness of methods by sampling

distinct random seeds during inference, or by downsampling features or cells (**Methods**).

To extend GRN benchmarking strategies beyond the recovery of TF binding peaks measured by ChIP-seq data and to incorporate the novel multimodal GRNs with distal CREs, GRETA offers a diverse collection of metrics grouped into three categories: mechanistic, predictive, and literature-based (**Fig. 2**). Detailed objectives and evaluation procedures for each metric are provided in **Table 1** and **Methods.** Mechanistic metrics evaluate whether GRNs capture causal relationships from perturbation assays by assessing two aspects: their ability to identify perturbed TFs using enrichment scores from gene signatures ("TF activity") and their accuracy in predicting gene expression changes after perturbation ("Forecasting") (**Methods**). Predictive metrics assess how well GRN topology models observational single-cell RNA-seq and ATAC-seq data ("Omics") and gene set enrichment scores ("Gene sets") (**Methods**). Literature-derived metrics measure the extent to which GRNs incorporate prior knowledge from databases, focusing on several aspects: inclusion of known TF markers ("Marker TFs"); TF-TF protein-protein interactions based on shared target genes ("TF-TF pairs"); TF binding events to CREs validated by independent ChIP-seq data ("TF binding"); CREs identified as functionally active through biochemical assays, evolutionary conservation, or genetic variant presence; and CREs linked to genes via expression quantitative trait locus (eQTLs) (**Methods**).

After processing all evaluation databases, we observed a high overlap of coverage for target genes, a moderate coverage for TFs, and a low coverage for overlapping genomic regions across resources (mean overlap coefficient genes = 0.7528; mean overlap coefficient TFs = 0.5382; mean overlap coefficient base pairs = 0.311)(**Extended Data Fig. 1a-c**).

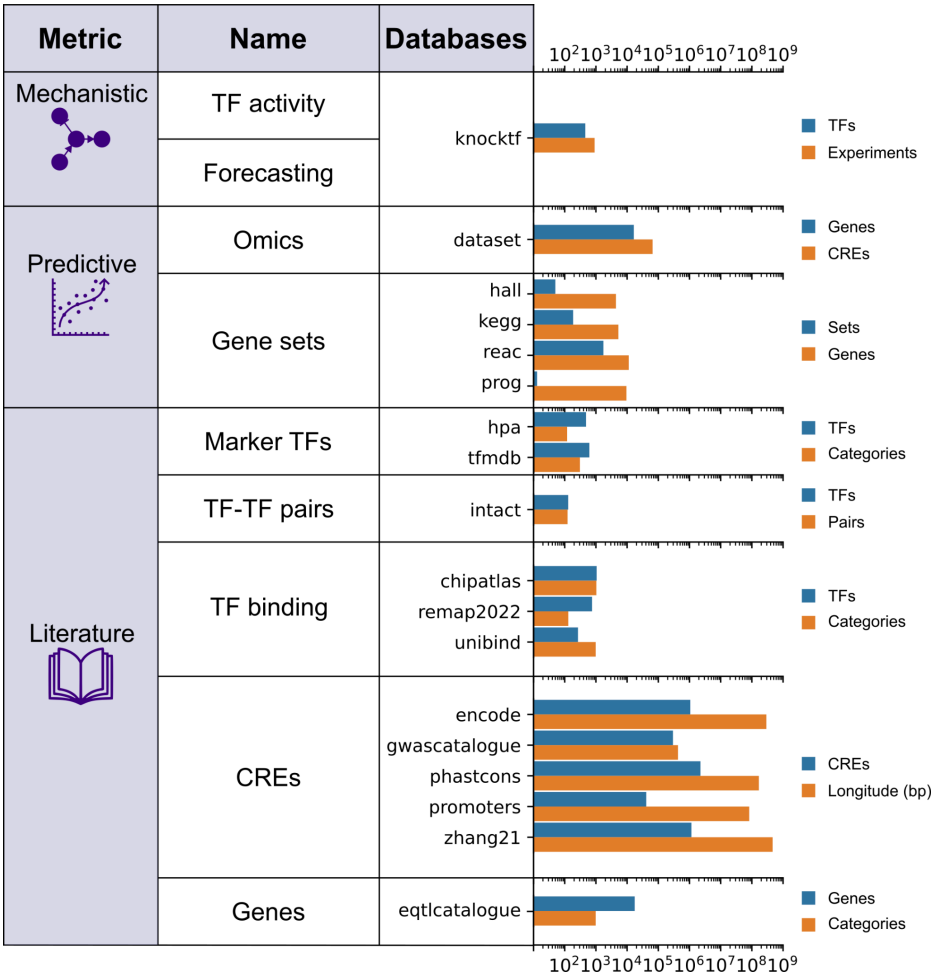

Figure 2. Evaluation metrics and processed databases. *List of evaluation metrics, the databases employed to calculate evaluation scores and their statistics such as number of elements, or number of cell-type or tissue labels. The Omics does not use a database as it used the original single-cell data.*

2.2. Systematic comparison and stability quantification of GRNs inferred from multiple methods

We used GRETA to reconstruct the GRN of a publicly available, annotated single-cell multiome dataset of human pituitary gland[21] using the original implementations of the five multimodal GRN reconstruction methods, *SCENIC*, two prior knowledge GRNs, and a random GRN (**Methods**).

First, we evaluated the robustness of the methods in reproducing GRN inference across three different random seed runs using the same pituitary dataset. Most methods consistently recovered the same TFs and target genes through each run

(mean overlap coefficient TFs = 0.96; mean overlap coefficient genes = 0.95), as well as their interactions (mean overlap coefficient edges = 0.85)(**Extended Data Fig. 2a**). However, *Dictys* and *SCENIC* showed substantial decreases in overlap of edges, with overlap coefficient values below 0.5 (**Fig. 3a**). Next, we evaluated the consistency of interaction weights across replicates for the methods that did not achieve a complete overlap (overlap coefficient = 1) across random seeds. Most methods showed strong correlations, reflecting stable interaction inference (median Pearson's ρ = 0.96) (**Extended Data Fig. 2b**). However, *Dictys* displayed correlation values below 0.5, with highly weighted TF-Gene interactions reversing their direction between runs. These findings suggest that the probabilistic nature of certain methods can affect GRN inference and impact downstream analyses.

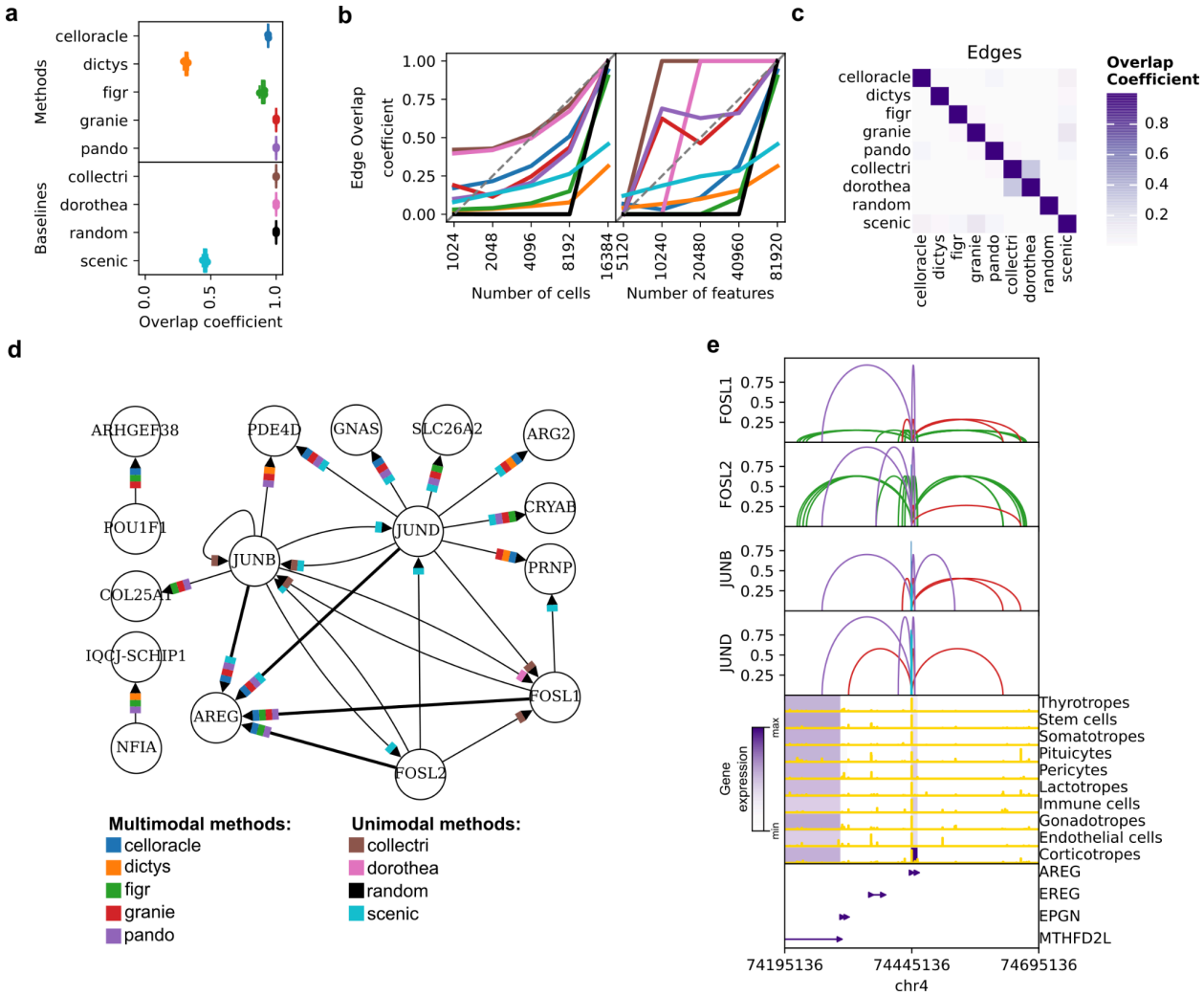

Figure 3. Stability and overlap of multimodal GRN inference methods. a*, Overlap coefficients of edges between three runs with different random seeds per method.* ***b****, Overlap coefficients of edges between GRNs inferred from increasingly downsampled datasets at the feature or cell level with the one inferred using the full dataset.* ***c****, Overlap coefficients of edges across methods.* ***d****, A shared network across multimodal GRNs with overlapping edges from the unimodal ones. Regulatory interactions to the AREG gene are highlighted by a wider link.* ***e****, Genomic neighborhood of AREG showing the gene annotations (bottom), the mean gene expression and chromatin accessibility of CREs across cell types (middle), and predicted TF-CRE interactions for AREG's TFs. Link heights indicate the quantile of the TF-Gene scores inside each method.*

We next examined how data size affects GRN reconstruction, since the number of cells or features retained from the same sampled tissue can vary depending on the experimental protocol, and the single-cell data processing framework and its

chosen parameters[22]. The pituitary gland dataset was progressively downsampled across four decreasing values in terms of the number of highly variable features or cells, and GRNs were inferred as previously described. For each downsampling level, three different random seeds were used. The resulting networks were compared to those generated from the full dataset at the TF, edge, and target gene levels using the overlap coefficient. A stability score was calculated based on the area under the curve of overlap coefficients, with values close to one indicating minimal impact to downsampling and values close to zero indicating substantial impact (**Methods**). Reducing numbers of cells and features did not drastically impact the recovery of TFs and genes, with a moderate reduction in overlap coefficients (mean stability score for TFs and genes = 0.73) (**Extended Data Fig. 2c,d**). However, we observed a sharp decline in similarity at the edge level across all methods (mean stability score = 0.35) (**Fig. 3b**, **Extended Data Fig. 2d**). Measurements of running times and memory usage during the subsampling strategy underlined the substantial computational resource requirements of multimodal methods (**Supplementary note 1**, **Extended Data Fig. 2e**). These findings show that data coverage strongly impacts network structure, especially interactions, emphasizing the need to optimize preprocessing to retain key network features.

Next, we compared the GRNs obtained from the same dataset with different methods. Most methods inferred GRNs with similar numbers of TFs, edges, and number of target genes per TF (median TFs = 245, edges = 2,663, genes = 1,569, regulon size = 17.3)**(Extended Data Fig. 3a)**. *Dictys* and *SCENIC*, however, produced much larger networks with over 20k edges, nearly 10k target genes, and regulons exceeding 50 genes. Additionally, methods linked genes to CREs that were located at different genomic distances, even though all methods were set to use the same distance parameter (± 250 kb from TSS[1]) (median CRE distance to TSS = 12,7 kb)(**Extended Data Fig. 3b**). In particular, *CellOracle* mostly only recovered promoter regions close to the TSS, while *Pando* sometimes identified distal interactions outside the distance limit. In summary, the GRNs obtained from different methods have substantial topological differences.

When comparing the overlap of the GRNs obtained with different methods, they showed moderate agreement at the TF and target gene levels (mean overlap coefficient TFs = 0.46; mean overlap coefficient genes = 0.45)(**Extended Data Fig. 3c**), but minimal overlap at the edge level (mean overlap coefficient edges = 0.02) (**Fig. 3c**). We also found notable differences between the distinct TSS annotations used across methods (mean genomic overlap coefficient = 0.7692)(**Extended Data Fig. 3d**). Particularly, annotations from *CellOracle* and *FigR* had the fewest overlaps to the others (mean genomic overlap coefficient *CellOracle* = 0.6377, *FigR* = 0.66). While the rest of methods use similar releases of Ensembl's hg38 gene annotation version[23], *CellOracle* uses a custom annotation inferred using Homer[24], and *FigR* uses hg19 RefSeq. These results show that, while these methods share similar inference steps, their algorithmic choices and use of prior knowledge influence GRN reconstruction.

Although the methods showed limited overlap at the edge level, for a small regulatory network involving the TFs FOSL1, FOSL2, JUNB, and JUND among others, each regulatory interaction was recurrent in at least three out of the five multimodal methods at a time (**Fig. 3d**, **Extended Data Fig. 3e**). GRN methods jointly identified *AREG*, a signaling ligand of the epidermal growth factor receptor[25], as a highly regulated target gene by these TFs. *AREG* was neither present in the literature-derived GRNs nor in the random network. While *SCENIC* captured some of these interactions, it inferred a larger number of edges compared to multimodal GRN methods, likely due to its exclusive reliance on transcriptomics, which may increase the likelihood of false positives. These results illustrate how GRN inference methods can uncover previously uncharacterized regulatory interactions.

To understand how different methods justified the regulatory links to *AREG* we visualized their predicted TF-CRE-Gene interactions on the genome (**Fig. 3e**). While *AREG*'s promoter region was accessible across all cell types, its expression was restricted to corticotropes, a pituitary gland cell type that secretes stress hormones upon hypothalamic stimulation[26]. This suggested that *AREG*'s expression was influenced by context-specific distal cis-regulatory interactions.

Comparing the CREs used by each method to support the same TF-Gene interactions revealed notable differences, illustrating variability in how methods infer regulatory links.

Altogether, the results in this section highlight variability in network size and connectivity across methods, reflecting differences in their inference steps and algorithmic strategies.

2.3. Evaluating the impact of paired vs unpaired multiome data in GRN inference

Another key element to consider when performing GRN inference is the nature of the multimodal data being used. Whether the data are truly paired, measuring both, snRNA-seq and snATAC-seq from the same cells, or unpaired, measuring them from different cells, has the potential to impact GRN reconstruction[27]. While some methods, such as *CellOracle* and *GRaNIE*, are designed to handle both paired and unpaired data, others are limited to paired data and rely on computational strategies to integrate the modalities when working with unpaired datasets. To evaluate the impact of these differences on GRN inference, we again used the human pituitary gland dataset, which uniquely includes profiles from the same donor generated with both paired and unpaired multiome technologies, making it particularly suitable for this comparison **(Fig. 4a).**

To integrate the unpaired dataset, we used *FigR*'s integration approach based on optimal transport, as it is one of the few methods that return a one-to-one mapping between barcodes (**Methods**). After identical processing, we observed that the paired and unpaired datasets were similar (**Extended Data Fig. 4a**), both at the level of cell type abundances (cosine similarity = 0.94) and molecular readouts (RNA mean Spearman ρ = 0.9586; RNA mean FDR < 2.2×10^{-16}; ATAC mean Spearman ρ = 0.7722; ATAC mean FDR < 2.2×10^{-16})(**Fig. 4b**). We also noticed that both runs had a similar sequencing depth and total number of features (mean log1p total counts = 8.01; mean log1p number of genes = 7.36)(**Extended Data Fig. 4b**). However, we found that the unpaired dataset showed a higher mean sequencing depth (two-sided Rank sums test, N per group= 10 cell types; W = 2.57;

BH FDR = 0.01) and mean number of features (two-sided Rank sums test, N per group= 10 cell types; W = 2.87; BH FDR = 0.0162) across cell types in snRNA-seq. We then compared the GRNs inferred from both datasets for each method, and we found low overlap between the edges of the networks (mean overlap coefficient edges = 0.14)(**Fig. 4c**). These results suggested that, while paired and unpaired multiome datasets retain global cell-type properties, the computational integration of unpaired data introduces differences that affect the inferred GRNs.

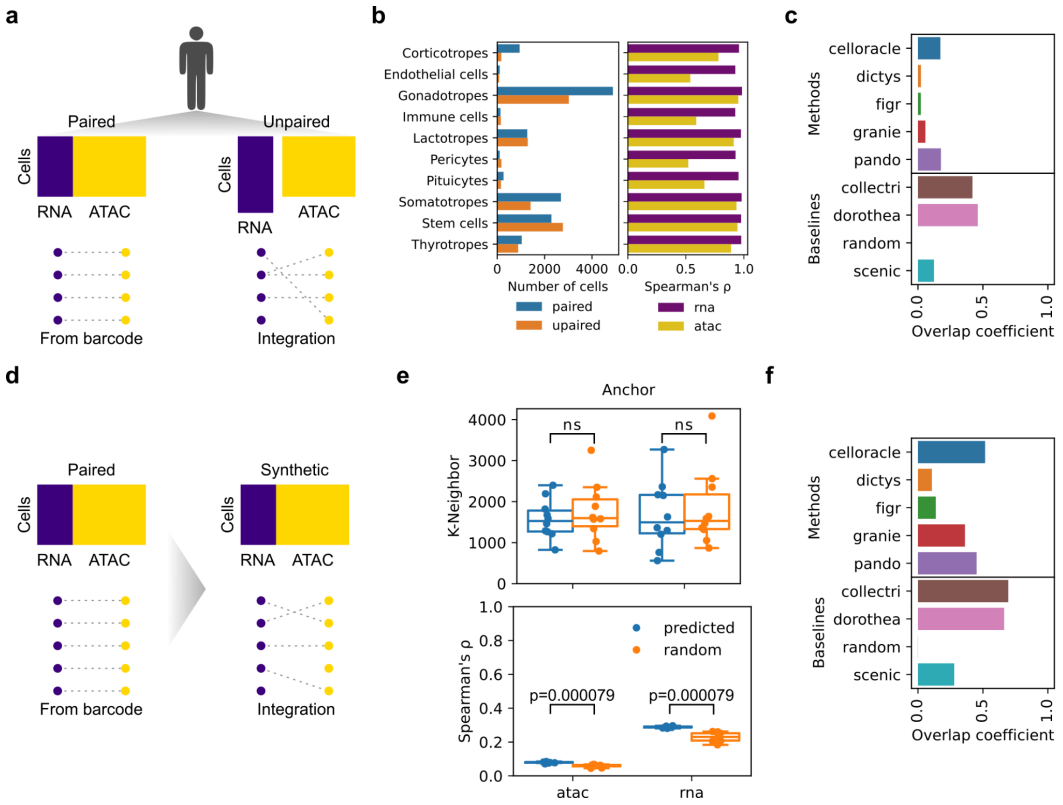

Figure 4 Impact of paired vs unpaired multimodal data in GRN inference. a*, Paired and unpaired single-cell multiomics were measured for the same pituitary gland. In paired data, the mapping between modalities cells is known, while in unpaired the number of cells can be different and requires integration between modalities. Missing or non-straight lines denote imperfect matching.* ***b****, Number of cells per cell type for both datasets (left), Spearman's ρ between the molecular readouts of the paired and unpaired datasets per cell type (right).* ***c****, Overlap coefficient of edges between the GRNs inferred from the paired and unpaired dataset.* ***d****, By treating the paired pituitary dataset as if it were unpaired, we created a synthetic integrated dataset by matching cells using FigR's integration approach. Missing or non-straight lines denote imperfect matching.* ***e****, Mean k-neighbour for each cell type of the predicted and random cells from the same cell type (top), and the mean Spearman ρ between the predicted and random cells across data modalities. Anchor refers to which modality was used in the obtained mapping to make the comparisons.* ***d****, Overlap coefficient of edges between the GRNs inferred from the paired and synthetic dataset.*

To assess the effects of data integration on GRN inference, we compared the original paired multiome pituitary dataset with a synthetic paired dataset, generated by treating the original data as unpaired and integrating it using FigR (**Methods**, **Fig. 4d**). Synthetic pairing correctly assigned only 87 cells to their

corresponding original cell from the paired information (0.63 % of total cells). Although integration generally paired cells across modalities within the same cell type **(Extended Data Fig. 4c)**, the assigned pairs were as distant from the original cell as randomly assigned pairs within the same cell type both at the RNA-seq (one-sided Rank sum test; median k-neighbor of predicted cells in RNA per cell type = 1,495.71; median k-neighbors of random cells in RNA per cell type = 1,530.25; N per group = 10 cell types; W = -0.378; P = 0.3527) and ATAC-seq (one-sided Rank sum test; median of k-neighbor predicted cells in ATAC per cell type = 1,527.31; median k-neighbor of random cells in ATAC per cell type = 1,597.78, N per group = 10 cell types; W = -0.453; P = 0.3251) (**Fig. 4e**) level. Nevertheless, synthetically paired cells showed a higher correlation of RNA and ATAC features compared to randomly assigned pairs within the same cell-type (one-sided Rank sum test; median Spearman's ρ of predicted cells in RNA per cell type = 0.2874; median Spearman's ρ of random cells in RNA per cell type = 0.23; N per group = 10 cell types; W = 3.7796; P = 7.85e-05)(one-sided Rank sum test; median Spearman's ρ of predicted cells in ATAC per cell type = 0.0795; median Spearman's ρ of random cells in ATAC per cell type = 0.0619; N per group = 10 cell types; W = 3.7796; P = 7.85e-05)(**Fig. 4e**). Comparison of GRNs from the paired and synthetic paired datasets revealed low overlap of interactions (mean overlap coefficient edges = 0.34; **Fig. 4f)**. These findings suggested that while integration accurately groups cells by cell type, it fails to align them within finer cell states, reducing the effectiveness of GRN methods that rely on paired multimodal data.

2.4. Decomposing multimodal GRN inference

To evaluate the impact of each inference step of multimodal methods in the reconstruction of GRNs, we used a paired multiome dataset of peripheral blood mononuclear cells (**Extended Data Fig. 5a-c**) and systematically replaced individual steps in each original method with those from other methods (**Methods**). To validate our implementations, we compared GRETA's decoupled version of multimodal GRN methods to the original ones. With the exception of *Dictys*, which showed instability of GRN inference in its own original implementation (**Results 2.2**), all other methods demonstrated high consistency,

with substantial edge overlap coefficients and Spearman's ρ between the original and GRETA implementations (mean edge overlap coefficient = 0.78; mean Spearman's ρ = 0.85) (**Extended Data Fig. 5d**).

We next combined the inference steps across methods and observed that replacing individual steps with those from other methods had varying impacts on GRN reconstruction. Across different combinations, overlap coefficients for TFs and genes included in the GRNs remained consistently above 0.5, although gene-level overlap showed greater variability (TF mean overlap coefficient = 0.8461; gene mean overlap coefficient = 0.7901; **Extended Data Fig. 5e-h**). However, at the edge level, modifying a single analysis step substantially altered the GRN structure, resulting in lower overlap coefficients (mean overlap coefficient = 0.2877; **Fig. 5a**).

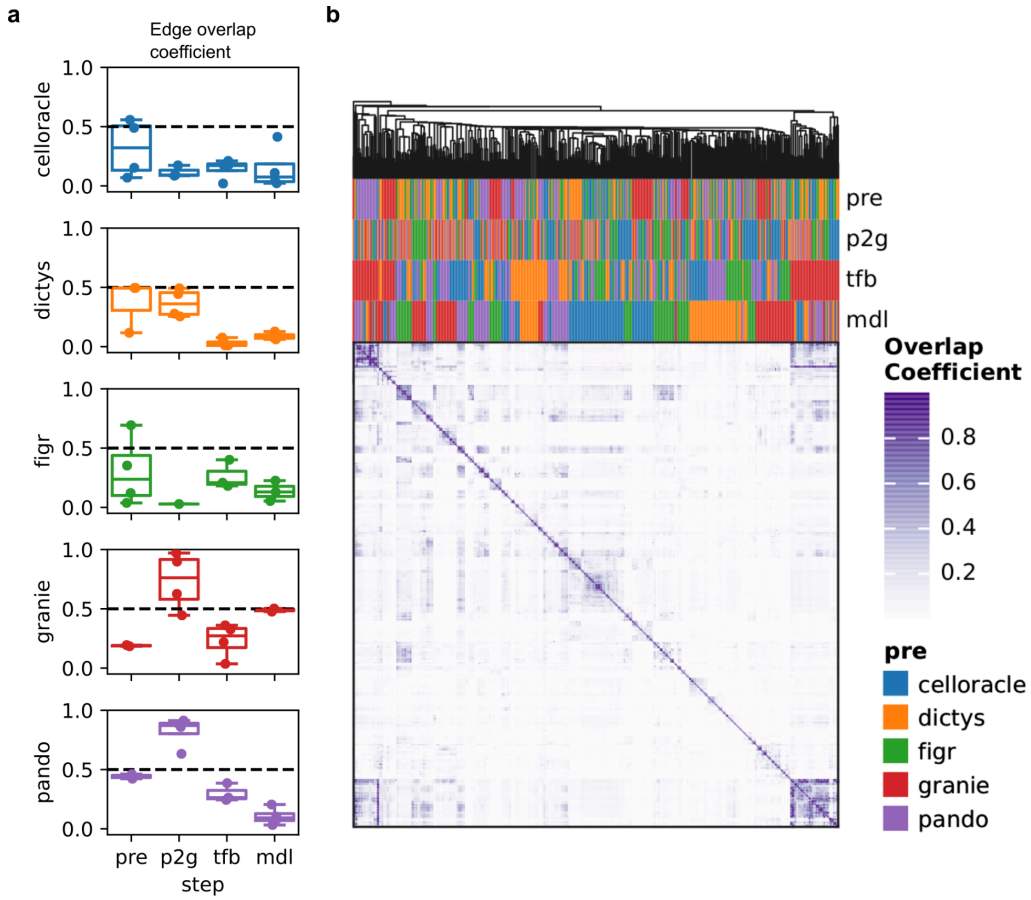

Figure 5. Multimodal GRN inference decomposition. ***a****, Effect of changing one of the inference steps from a fixed method pipeline to another method, measured by the overlap coefficient at the edge level.* ***b****, Pairwise overlap coefficient at the edge level between all possible inference runs combinations.*

We next examined whether different runs would converge to a limited set of solutions. To assess this, we performed all possible runs (4^N, where N was the number of multimodal GRN methods) and clustered them based on pairwise overlap coefficients at the TF, edge, and gene levels. Based on the overlap of TFs and genes used in the GRN, methods clustered according to the TF binding and CRE-to-gene steps, respectively (mean TF overlap coefficient = 0.6597; mean gene overlap coefficient = 0.5304)(**Extended Data Fig. 5**). However, when comparing the similarity of GRN interactions across different inference step combinations, edge-level overlap coefficients were only marginally higher than those observed for random GRNs (mean non-random overlap = 0.071; mean random overlap = 0.0026; **Fig. 5b**). This suggests that although methods incorporate similar TFs and

genes, each combination of them generates a unique solution to the inference problem.

2.5. Evaluation of multimodal GRNs

To assess the performance of combinations of steps and original multimodal methods, we used the evaluation metrics defined in **Fig. 2** and **Table 1**, applied to the different runs obtained in **Fig. 5**. For each metric and GRN, precision and recall were calculated based on the metric-specific definitions of true positives (TPs), false positives (FPs), and false negatives (FNs)(**Table 1**). These values were summarized into an F score, with precision weighted ten times more than recall ($\beta = 0.1$), denoted F_{01}. This weighting was chosen because GRN inference methods typically return sparse networks that prioritize precision, as they aim to capture the most confident interactions rather than all possible ones in the ground truth [15]. Given that the ground truth is not perfect, precision becomes more important than recall to ensure the predictions accurately reflect the true regulatory interactions. A weighted Kolmogorov-Smirnov-like statistical test was then used to identify method steps that ranked significantly higher based on the F_{01} score (**Methods**, FDR < 0.01)(**Fig. 6a**).

Most GRNs had a moderate performance at recapitulating findings of literature (mean F_{01} score = 0.328), including TF markers, TF-TF interactions via shared targets, validated TF binding events, functional CREs identified through assays or conservation, and CRE-gene links supported by eQTLs (**Table 1**). Among the methods evaluated, specific approaches performed better in distinct tasks (**Extended Data Fig. 6**). *FigR*'s modeling strategy performed better in tasks related to the HPA database (mean F_{01} score = 0.4631), while *GRaNIE*'s TF binding approach showed higher performance across all TF binding databases (mean F_{01} score ChIP-Atlas = 0.21, Remap2022 = 0.3445, UniBind = 0.2074). For CRE-related tasks, *Pando*'s preprocessing strategy performed best for evolutionary conservation (mean F_{01} score = 0.7909), while *CellOracle*'s CRE-to-gene strategy performed better in tasks involving the GWAS catalog (mean F_{01} score = 0.00087), promoters (mean F_{01} score = 0.6123), and the recovery of CRE-gene links (mean F_{01} score = 0.2301).

Lastly, *Dictys*' modeling strategy, TF binding approach, CRE-to-gene, and preprocessing strategy, scored the highest in TF-TF pairs (mean F_{01} score = 0.3222), TF-Marker resource (mean F_{01} score = 0.5125), ENCODE (mean F_{01} score = 0.8351), and Zhang (mean F_{01} score = 0.8596) resources respectively.

Similarly, most methods performed decently on prediction tasks (mean F_{01} score = 0.516), where the objective is to evaluate the prediction of gene expression, regulatory elements accessibility, or biological processes using the network topology (**Table 1**). *Dictys*' modeling strategy achieved the highest scores across all omics tasks (mean F_{01} score Gene ~ TFs = 0.6211, CRE ~ TFs = 0.5367, Gene ~ CREs = 0.6211), whereas *CellOracle*'s modeling strategy outperformed others in all gene set databases (mean F_{01} score Hallmarks = 0.61, Kegg = 0.6381, Reactome = 0.6544, PROGENy = 0.7066) (**Extended Data Fig. 6**).

All method combinations performed poorly in mechanistic tasks (mean F_{01} score = 0.0395), aimed at predicting the effects of perturbing TFs (**Table 1**). However, among the methods *GRaNIE*'s TF binding approach performed best for predicting TF activities (mean F_{01} score = 0.0515), while *CellOracle*'s modeling strategy ranked higher at forecasting changes in gene expression (mean F_{01} score = 0.0417) (**Extended Data Fig. 6**).

When evaluating the performance of methods at each inference step, the preprocessing strategy of *Dictys*, the CRE-to-gene strategy of *Dictys* and *Pando*, the TF binding strategy of *Dictys* and *GRaNIE*, and the modeling strategy of *Dictys* and *CellOracle* achieved higher F_{01} scores across more tasks compared to other strategies (**Fig. 6b**).

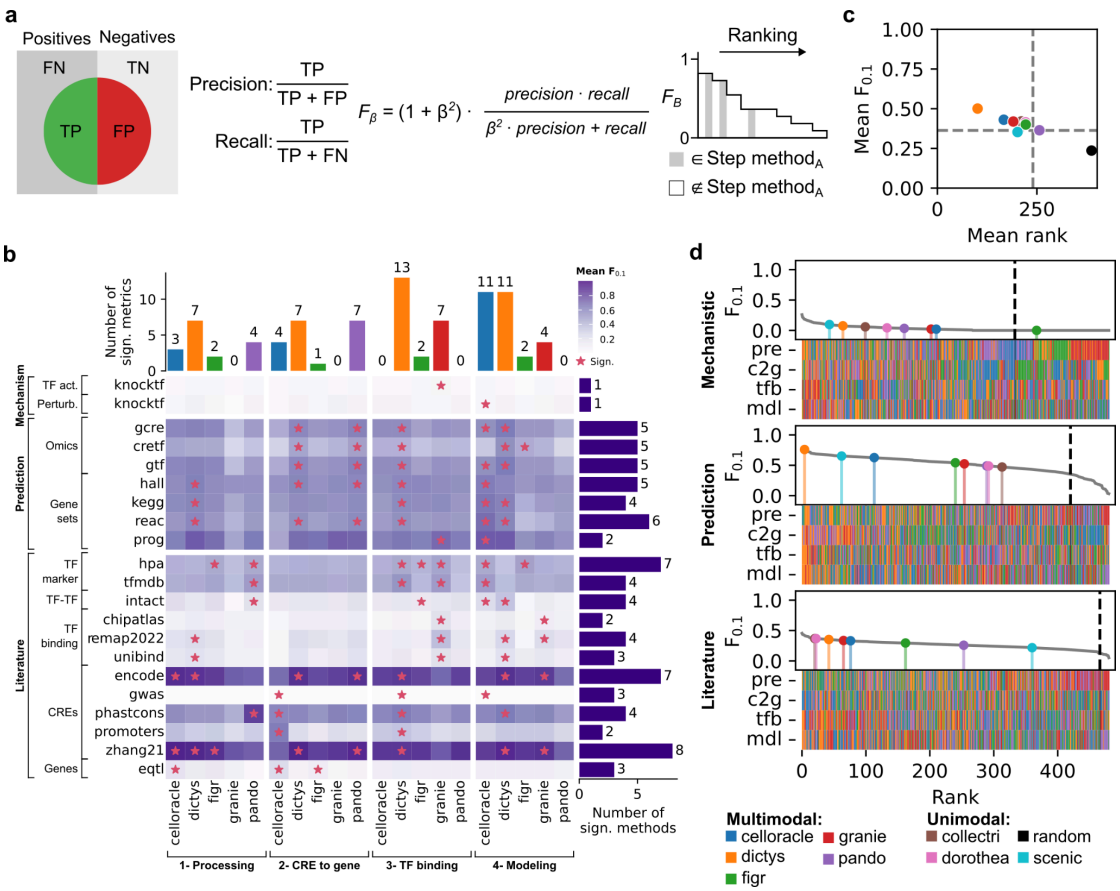

Figure 6. Multimodal GRN evaluation. ***a****, Strategy used to assess the performance of each GRN inference step across metrics. Precision and recall were first computed from true positives (TPs), false positives (FPs), and false negatives (FNs). These were then summarized into an F_β score, with precision weighted ten times more than recall (β = 0.1). A running score statistical test was used to assess whether groups of runs sharing a specific method's inference step were ranked significantly higher than others.* ***b****, Mean $F_{0.1}$ scores across evaluation metrics and inference steps per method plus the unimodal GRN methods. Asterisks indicate that runs using a method's step ranked significantly higher than the rest for a particular metric. Barplots indicate the number of significant method-metric pairs grouped per method's step (top) or per metric (right).* ***c****, Averaged $F_{0.1}$ scores based on the three metric categories per individual run. Lollipop plots indicate fixed pipelines, and color indicates the different methods. The dashed line indicates the random GRN.*

Next, we compared the ranks of the fixed original multimodal pipelines and the unimodal methods against all possible combinations of runs across the evaluation metrics. We found that all methods outperformed both the mean rank and F_{01} score of all method combinations (**Fig. 6c**), except for *Pando*, *SCENIC* and the

random baseline (mean rank all combinations = 239.97, *Pando* = 256.28, SCENIC = 201.33, random = 387.19; mean F_{01} score all combinations = 0.3632, *Pando* = 0.3644, *SCENIC* = 0.353, random = 0.2362). Notably, *Dictys* outperformed the other fixed methods, as it had the lowest mean rank (mean rank = 101) and higher mean F_{01} score (mean F_{01} = 0.501).

We then evaluated the performance of the fixed runs across the three metric types (**Fig. 6d**, **Extended Data Fig. 7a**). *Dictys* and *SCENIC* achieved the highest mean F_{01} scores in both mechanistic and predictive metrics. In contrast, *CollecTRI* and *DoRothEA* ranked highest in literature-based metrics, followed by *Dictys*, while *SCENIC* performed poorly in this category.

Given that *Dictys* produced anticorrelated results across different runs (**Extended Data Fig. 2b**), we evaluated its stability in performance by running it with five different random seeds (**Extended Data Fig. 7b**). The results showed that the obtained F_{01} scores were consistent (mean standard deviation = 0.0305), suggesting that *Dictys* may identify multiple optimal local minima.

3. Discussion

The accumulation of single-cell datasets profiling both transcriptomics (snRNA-seq) and chromatin accessibility (snATAC-seq) has spurred the development of several methods that integrate these data to infer gene regulatory networks (GRNs). These networks link transcription factors (TFs) to accessible cis-regulatory elements (CREs) that regulate neighboring genes. To systematically compare and evaluate these methods, we built GRETA, a framework that integrates and decouples the inference steps from multiple multimodal GRN inference methods, as well as some unimodal ones. Using GRETA, we explored the stability and agreement among these methods and their inference steps, their sensitivity to the type of multimodal data used during inference, and their performance across different tasks.

Our results show that these methods have limited robustness, yield substantially different outcomes from one another and are affected by the type of multimodal

data being used. Moreover, even within the limited shared regulatory interactions, we observed differences in which cis-regulatory interactions methods use to make their TF-gene TF-gene predictions using the same data. These differences likely stem from the distinct empirical decisions made during GRN inference, as well as variation in the prior knowledge resources and genome annotations used by each method. Such limitations in current methods complicate the evaluation of novel interactions, as technical variability outweighs biological signals.

Multimodal GRN inference method implementations are complex, often requiring diverse input data formats and challenging installations, with advanced coding skills needed to use them effectively. Additionally, their computational costs are high, so that users require access to high-computing clusters, limiting their accessibility to a broader community. GRETA reduces these barriers by offering a modular pipeline that simplifies workflows, supports reproducibility, and facilitates systematic comparisons and novel combinations of GRN inference steps.

Our analysis of the pituitary paired and unpaired multimodal datasets revealed that, although the two datasets were similar at the cell abundance and molecular levels, the inferred GRNs were substantially different. Single-cell multiomics integration remains a challenging problem that has not yet been fully solved[27]. For instance, in RNA and ATAC integration, CREs are transformed into genes by computing gene scores based on gene promoter accessibility[28], which are then used to match the two modalities at the gene level. While this strategy may successfully map cells to their matching cell type, promoter accessibility does not necessarily guarantee gene expression[1], making the mapping of cells to specific cell states a difficult task. Specifically, we observed that cells from the same cell type already exhibit low correlation with each other, suggesting that fine mapping of 1-to-1 cells might be unreachable. Consequently, paired data should be employed whenever possible to improve the accuracy of cell state mapping and GRN inference.

We showed that the topology of GRNs can moderately predict the levels of gene expression in terms of their regulatory elements, and recapitulate partially the regulation of biological processes and literature. However, their performance is not

substantially better from unimodal methods, except for *Dictys*. However, all methods performed poorly in TF perturbation tasks. The lack of causal properties raises the question of which other modalities or technologies we need to achieve reliable trans-regulation predictions. This finding is consistent with other evaluation efforts, which have shown similar challenges for classic regression models[29] and the new wave of deep-learning and foundation models[30]. Estimating causal relationships observed in perturbation data from GRNs built from observational data is intrinsically a challenging problem[31]. This difficulty is compounded with the fact that the process of trans-regulation involves multiple steps that are not fully captured by gene expression or chromatin accessibility data alone. For a TF to regulate a target gene, its transcript must first exit the nucleus via nuclear pores, be translated into protein, undergo activation through post-translational modifications, re-enter the nucleus, interact with other nuclear TFs, and interact with accessible chromatin and favorable conditions at the target transcription start site (TSS) to exert regulatory effects. This complex chain of events is further complicated by processes we may not yet fully understand or have not yet discovered. Promising experimental approaches to improve GRN inference include systematic perturbation at scale[32], TF dosage dynamics[33], or joint spatial 3D accessibility of chromatin with protein staining[34]. From the modeling side, sequence-based models that predict genomic molecular readouts such as chromatin accessibility could be incorporated into GRN inference methods[35], as they can refine the TF binding step to be context specific.

Although this is, to the best of our knowledge, the most comprehensive attempt to systematically evaluate multimodal GRN inference methods, benchmarking remains a challenging task due to the elusive nature of ground truth[11,36]. Another limitation is that, except for the predictive metrics, all other metrics rely on context-specific databases. This limitation prevented us from evaluating the pituitary dataset, as few databases had entries for this organ. Additionally, our current work is limited by the number of datasets and methods we used. We are in the process of incorporating additional datasets and other methods[11]. A further limitation is that our study is currently focused only on human data. Given the

availability of extensive data for model organisms such as mouse[37] or fly[38], it could be expanded to evaluate the generalizability of our findings to these organisms.

In summary, we present a framework to facilitate the inference, comparison and benchmarking of GRNs from single-cell multiomics data, providing results that help understand the strengths and weaknesses of existing methods. With it, we show that inference choices drastically affect the results, highlighting the need for greater focus on the robustness of these methods. We envision GRETA as a collaborative project, where we welcome others to use or contribute to the framework (GRETA: https://github.com/saezlab/greta), to advance together the GRN inference field.

4. Methods

snMultiome data processing

Raw transcript count matrices, sample-specific chromatin accessibility fragment files and global barcode annotations were retrieved for each dataset from GEO, CELLxGENE and 10x Genomics portal. Fragment files were processed to assign the corresponding sample names to barcodes, ensuring that they were unique. Each dataset was processed independently using the same processing pipeline described below.

For each sample in a dataset, fragment files were processed into tile matrices using SnapATAC2[39]. Barcodes not present in each dataset annotation metadata were removed, guaranteeing that only good quality barcodes were kept. Tile matrices were concatenated and dataset-specific consensus accessibility peaks (Cis-Regulatory Elements, CREs) were called using SnapATAC2's implementation of MACS3[40].

Genes expressed in few cells were removed from transcript count matrices, and cells containing few expressed genes, and (number of genes > 100, number of cells > 3). Gene symbols from transcript count matrices were removed if not present in Ensembl 111[23]. For each dataset, if a gene symbol appeared more than once, the

feature with counts detected in the highest number of cells was kept. Barcodes were only kept if they were present in the corresponding dataset annotation. Then, transcript and accessibility matrices were paired into a MuData object[41].

Genes or CREs with low detection were removed (number of counts detected per barcode ≤ 3). For each omic, counts were normalized by barcode-specific total counts (target sum = 1e4) and log1p transformed with scanpy[42]. Feature selection was performed by calculating highly-variable features for each sample and then keeping the top number of features that were found to be variable in the maximum number of samples (number genes = 2^{14}, number CREs = 4 x 2^{14}).

Simultaneous dimension reduction using Laplacian Eigenmaps was computed with SnapATAC2. For multi-sample datasets, the obtained spectral embeddings were integrated across samples using harmony-py until convergence[43]. With the corrected embeddings, a neighborhood graph of barcodes was inferred, followed by UMAP dimensionality reduction for visualization purposes. Original raw integer counts for genes and CREs were kept in the layers of the MuData object for downstream analyses.

snRNA-seq and snATAC-seq pairing

To integrate the unpaired snRNA-seq and snATAC-seq pituitary datasets, we first generated a shared co-embedding using Seurat[44]. For the RNA data, we performed log normalization, selected highly variable genes, and scaled the data. For the ATAC data, we applied term frequency-inverse document frequency normalization, selected highly variable CREs, and scaled them as well. Gene scores were inferred from ATAC data and subsequently processed as RNA. Canonical correlation analysis was then used to derive the shared embedding between RNA and inferred gene scores. Individual cells were paired in a one-to-one manner using *FigR*'s integration approach based on optimal transport. Finally, the matched barcodes were merged into a paired MuData object. The same procedure was used to generate the synthetic paired dataset from the real paired pituitary dataset.

Original multimodal GRN inference methods implementation

This section explains how each multimodal GRN inference method was applied to each dataset, following the original developers' recommendations as closely as possible.

Following the documentation of *CellOracle* (v0.16.0)[14], Cicero[45] was used to identify CRE-CRE co-accessibility interaction scores with a window size around the transcription starting site (TSS) of 500 kb. CREs were annotated to genes if they were located at its TSS, using a custom annotation generated with Homer[46]. Pairs of CRE-TSS interactions were removed according to their interaction score (score < 0.2). For the remaining CREs, TF binding predictions were computed with the motif matcher algorithm GimmeMotifs[47] and the motif database CIS-BP[48] (FPR = 0.02, background length = 200 bp, $-\log_{10}$(FDR) > 10). CRE-gene and TF binding results were merged to obtain a scaffold TF-CRE-Gene network. K-Nearest Neighbours (KNN) was performed on the PCs of the gene expression matrix to reduce its sparsity (k = 20). Finally, a single tissue-level GRN was inferred with a Bagging Ridge linear model (alpha = 10, number of top significant edges = 2k).

Dictys (v1.1.0)[15] started by performing a basic quality control filtering (minimum total read count per gene > 50; minimum number of cells expression each gene > 10; minimum total read counts per cell > 200; minimum number of non-zero genes per cell > 100). Then, CRE were linked to neighboring genes based on genomic distance using Ensembl's (release 107) gene annotation[23] (window size = 500k). Wellington[49] and Homer[46] were then applied to identify TF footprints and enriched TF binding sites from HOCOMOCO v11[50] within the accessibility profiles of each pre-defined cluster. TFs were assigned to CREs by aggregating results from both methods, and the outcomes were averaged across clusters. The CRE-gene and TF-CRE associations were merged to obtain a scaffold TF-CRE-Gene network. Finally, a GRN was inferred by predicting gene expression using stochastic process models, retaining only interactions with |score| > 0.25.

For *FigR* (v0.1.0)[16], CRE-Gene interactions were inferred by computing the Spearman's correlation between the log-normalized gene expression and genomic

neighboring CREs accessibility counts (window size = 500k, FDR < 0.1, number of CREs per gene ≥ 2, hg19 RefSeq TSS annotation). Domains of regulatory chromatin (DORCs) scores were computed per gene by summing the accessibility counts of its associated CREs. Both DORC scores and log-normalized gene expression were smoothed using KNN imputation, leveraging SnapATAC2's spectral embeddings (k = 10). For each DORC, the method identified its k nearest neighbors based on the smoothed DORC scores and pooled their associated peaks. It then calculated TF binding frequencies for these pooled peaks with the MOODs[51,52] motif matcher algorithm and the CIS-BP[48] motif database, which were compared to a GC-corrected permuted background set (n = 50) using a z-test to assess significance. For the normalized gene expression, the Spearman's correlation was calculated between TF expression and DORC accessibility scores. A final regulation score was determined by combining the significance values of the TF–DORC correlation and TF binding prediction, with activation or inhibition assigned based on the sign of the correlation.

For *GRaNIE* (v1.9.7)[17], pseudo-bulk profiles at the cell-type level were generated for both omics using decoupler-py[53]. Genes were normalized with the quantile normalization from limma[54], and CREs with the size factors from DESeq2[55]. TF-CRE links were extracted by first overlapping predicted TF binding regions from HOCOMOCOv3[50] with PWMscan[56] to all CREs and then computing Pearson's correlation between normalized gene expression and chromatin accessibility. Similarly, CRE-Gene links were inferred by first assigning CREs to neighboring genes based on genomic distance and computing the Pearson correlation between pairs (window size = 500k). Finally, the two types of connections were merged and filtered for significance (TF-CRE FDR < 0.2, CRE-Gene < 0.2).

For *Pando* (v1.0.5)[18], CREs were redefined to only include base pairs present in evolutionary conserved regions from phastCons[57] and not present in annotated exonic regions. TF were assigned to CREs using TF motifs from JASPAR[58] and CIS-BP[48] with MOODs[51,52]. CREs were assigned to neighboring genes with the GREAT algorithm[59] (window size = 500kb). Then, multivariate generalized linear models were fitted for every gene explained by the interaction of the accessibility

of an assigned CRE with the expression of a TF assigned to that CRE. This was only done for features with enough TF-CRE or Gene-CRE Pearson's correlations (|Pearson| > 0.05). Finally, coefficients were filtered for significance, summed to the TF-Gene level and filtered by minimum number of targets (FDR < 0.1, R2 > 0.05, module size > 3).

Stability score

For features and cells, a stability score was computed for the TFs, edges, and gene overlaps coefficients across the decreasing downsampling iterations. This score was generated for each method by calculating the area under the overlap coefficient curve (AUC). The AUC was determined using the trapezoidal rule applied to a normalized sequence of downsampling steps ranging from 0 to 1, with five steps, and the corresponding overlap coefficient values for that method. This approach provides a quantitative measure of the GRN method's stability when downsampled by the number of cells or features.

Unimodal GRN inference methods

This section describes the GRN methods that do not directly model multimodal data, but still can incorporate CRE information through prior knowledge.

Literature-derived GRNs, *CollecTRI*[9] and *DoRothEA*[8], were obtained from their Zenodo[60] and GitHub repositories, respectively. For each dataset, non-expressed genes were removed from the GRNs. Then, a CRE was added for each gene comprising its promoter region (± 1kb from the TSS defined by Ensembl 111[23]). Finally, TF regulons were retained only if they contained more than five target genes.

SCENIC[19] first classified genes as TFs or non-TFs using a custom annotation provided by the method. For each gene, it then fitted an XGBoost model to predict its observed expression based on the expression of TF genes. Next, target genes within each TF regulon were pruned based on TF motif binding enrichment at their promoter regions. Finally, interactions were filtered by score, retaining only those with a score > 0.001.

For each dataset, a random GRN was generated by sampling 25% of the expressed genes at random. For each sampled gene, neighboring accessible CREs were selected within a 500 kb window based on the TSS annotation from Ensembl 111[23], using an exponential distribution (scale = 1). For each sampled CRE, annotated TFs from Lambert's database[61] that were also present in the sampled genes were similarly sampled using an exponential distribution (scale = 1). The resulting elements were merged, and TF regulons were randomly subsampled to achieve a TF-to-gene ratio of 10%.

Decoupled multimodal GRN inference methods

For each original method, we implemented a decoupled version designed to be compatible with other inference steps. While these individual steps largely mirrored the original implementations, minor modifications were made in some of the approaches to ensure maximum compatibility across different combinations of methods.

For *CellOracle*, accessibility imputation based on proximities in UMAP coordinates was not performed during CRE-CRE interaction inference with Cicero, as distances in UMAP space have no meaning[62].

For *Dictys*, datasets preprocessed using alternative strategies also incorporated *Dictys*' approach to reduce potential sparsity. Furthermore, when building the scaffold GRN prior to modeling, only peaks identified in the CRE-gene association step were included.

For *GRaNIE*, CRE-to-gene associations were performed first, followed by TF binding predictions within those associated CREs, rather than all available CREs. This approach was adopted because many peaks with TF binding predictions in the original implementation were ultimately excluded during the CRE-to-gene merging step. Additionally, the decoupled pipeline required a sequential processing order.

Similarly, for *Pando*, the processing order was adjusted from the original implementation: CRE-gene associations were performed first, followed by the TF

binding step. Additionally, to ensure compatibility with *FigR*, negative -log(p-values) obtained from MOODS were set to zero in the rare instances where they occurred.

Infrastructure

All Python-based methods were executed on a high-performance computing cluster using 32 cores, with a maximum memory allocation of 128 GB per step. R-based methods were restricted to a single core, as parallelization was observed to be slower and caused excessive memory consumption. To optimize runtime, individual steps in the decoupled pipeline were allowed a maximum execution time of nine hours; steps exceeding this limit returned an empty GRN. Additionally, combinations of steps that failed to produce valid CRE-gene associations, TF binding predictions, or TF-gene predictions also resulted in empty GRNs.

Evaluation metrics

For the mechanistic metrics, log fold changes and their associated metadata from single-TF perturbations were retrieved from KnockTF [63,64]. For the "TF activity" metric, perturbation experiments were filtered based on terms related to the dataset being evaluated (see https://github.com/saezlab/greta/blob/main/config/prior_cats.json). If a perturbed TF was present in the GRN, TF enrichment scores were inferred using decoupler-py's ULM method [53]. A perturbation was considered a true positive (TP) if the obtained enrichment score was both positive and significant (BH FDR < 0.05). For the "Forecasting" metric, assays were similarly filtered by matching terms. When a TF was present in the GRN, the effect of the perturbation was simulated by first averaging gene expression values across all cells from the original single-nuclei multiome dataset and then performing in silico perturbation simulations using CellOracle's perturbation framework (number of steps = 3). Perturbations were considered TPs when the Spearman's correlation between the simulated changes and the measured changes was significant ($\rho > 0.05$; BH FDR < 0.05).

For the predictive metric “Omics,” cells from the original single-nuclei multiome dataset were stratified by cell type, sampled, and split into training and testing sets (train size = 66%, test size = 33%). XGBoost was then used to model the following relationships: Genes ~ TFs, Genes ~ CREs, and CREs ~ TFs. Log-normalized gene expression was used for genes and TFs, while log-normalized chromatin accessibility was used for CREs. After fitting the models, predictions were made on the test set. Features were considered true positives (TPs) if the Spearman correlation was significant ($\rho > 0.05$; FDR < 0.05).

For the predictive metric “Gene sets,” several collections of gene sets were compiled, including Hallmarks[65], Kegg[66], Reactome[67] and PROGENy[68]. To identify relevant gene sets in the original single-nuclei multiome dataset, gene set enrichment scores were inferred at the cell level using decoupler-py's ULM method [53] and filtered for significance (minimum proportion of cells = 20%; enrichment score > 0; BH FDR < 0.01). For each TF in the GRN, a one-sided Fisher’s exact test was performed to determine which gene sets were overrepresented among its targets (BH FDR < 0.01). A gene set was considered a TP if it was overrepresented in at least one TF regulon within the GRN and was also significant in the original dataset.

For the literature-derived “TF marker” metrics, data from the Human Protein Atlas (HPA)[69] and TF-Marker[70] databases were retrieved. Entries from HPA were retained if the protein was annotated as a TF in Lambert[61], had evidence at the protein level, contained the word "Nucle" in their subcellular location, and was not non-specifically expressed across tissues, cell lines, or single-cell clusters. Both databases were further filtered based on terms relevant to the dataset being evaluated. A TF was considered a true positive (TP) if it was present in both the GRN and the database.

For the literature-derived “TF-TF pair” metric, protein-protein interactions were extracted from IntAct [71]. Interactions were retained if both proteins were annotated as TFs in Lambert[61] and had a high confidence score (MIscore > 0.75). For a given GRN, TF-TF pairs were identified by testing whether their target genes were

overrepresented with respect to each other using a one-sided Fisher's exact test (BH FDR < 0.01). A TF-TF pair was considered a true positive (TP) if it was present in both the GRN and the database.

For the literature-derived "TF binding" metric, we processed three large databases of ChIP-seq measurements: ChIP-Atlas[72], Remap2022[73] and Unibind[74]. From ChIP-Atlas, significant ChIP-seq TF binding peaks were retrieved for the TFs annotated in Lambert[61](BH FDR < 1e-50; maximum peak length < 750). From Remap2022, the non-redundant ChIP-seq TF binding peaks were retrieved for the TFs annotated in Lambert[61](maximum peak length < 750). From UniBind, ChIP-seq TF binding peaks from the robust collection were retrieved for the TFs annotated in Lambert[61](maximum peak length < 750). For each database, overlapping peaks from the same TF were merged using bedtools[75]. For a given dataset and GRN, TF binding databases were filtered to include only ChIP-seq peaks overlapping measured CREs from the original chromatin accessibility data using pyranges (v0.1.2)[76], TFs expressed in the original gene expression data, and cell type or tissue terms relevant to the dataset being evaluated. A TF binding peak was considered a TP if it overlapped with a CRE regulated by that TF according to the GRN.

For the literature-derived "CREs" metric, two enhancer annotation (ENCODE[77] and Zhang21[78]), an evolutionary conservation (PhastCons[57]) and a SNP-trait (GWAS catalog[79]) databases were processed. Additionally, a promoter resource was generated by opening genomic windows on the TSS annotated by Ensembl 111[23] (± 1kb from the TSS). For a given dataset and GRN, CRE databases were filtered to include only regions overlapping measured CREs from the original chromatin accessibility data using pyranges (v0.1.2)[76]. A CRE was considered a TP if it overlapped with a CRE in the GRN.

For the literature-derived "Genes" metric, eQTL Catalogue[80] was processed. CRE-Gene interactions were kept if the gene was annotated in Ensembl 111[23] and the link was significant (FDR < 1e-5). For a given dataset and GRN, the database was filtered to include only genes expressed in the original gene expression data, and cell type or tissue terms relevant to the dataset being evaluated. A CRE-Gene link

was considered to be a TP when the interaction was present in both the GRN and the dataset.

Statistical testing

Statistical tests were performed using scipy (v1.14.1)[81] and decoupler (v1.8.0)[53]. For false discovery rate (FDR) correction, the Benjamini-Hochberg (BH) procedure was employed.

In the evaluation of the decoupled GRN inference runs, to test for significantly ranked approaches the Weighted Kolmogorov-Smirnov-like statistic was repurposed from GSEA[82] using decoupler's implementation. In this case, the ranking value was the distribution of F_{01} scores across decoupled runs for a particular metric-database. The set of interest were the runs containing that specific inference step, for example all runs with TF binding prediction from *Dictys*, and the background were all the runs without that specific step (runs without the TF binding prediction from *Dictys*). By computing the Weighted Kolmogorov-Smirnov-like statistic, an enrichment score was obtained which was tested using random permutations of background runs (number of permutations = 1000). Significance was assigned based on the sign of the enrichment score (score > 0; BH FDR < 0.01).

Plots and figures

Plots were generated using the matplotlib (v3.9.2)[83], seaborn (v0.13.2)[84] and marsilea(v0.3.2)[85] libraries. Figures were then edited with Inkscape.

5. Acknowledgements

Thanks to Christian Arnold, Seppe de Winter, Adam Kyle, Philipp Sven Lars Schäfer, Aryan Kamal, Jalil Nourisa, Anshul Kundaje, Judith Zaugg, Stein Aerts, Carl Herrmann, Yvan Saeys, and Ingrid Lohmann for helpful discussions about gene regulatory networks.

SMD was supported by the German Federal Ministry of Education and Research, particularly the LiSyM Cancer research core (BMBF, Funding number: 031L0257B). The authors acknowledge support by the state of Baden-Württemberg through bwHPC and the German Research Foundation (DFG) through grant INST 35/1597-1 FUGG.

6. Conflict of interests

PBM is partially supported by funding from GSK. JSR reports funding from GSK, Pfizer and Sanofi and fees/honoraria from Travere Therapeutics, Stadapharm, Astex, Pfizer, Grunenthal, Moderna, Tempus, and Owkin.

7. Authors contributions

PBM, RRF and JSR conceived and designed the study. PBM, LW and SMD searched and processed the single-cell multiome datasets. PBM, RCF, LW and RRF searched and processed the evaluation databases. PBM, RCF, RT and YY implemented the multimodal gene regulatory inference methods. PBM performed the computational analyses, supervised by RRF and JSR. PBM, RRF and JSR wrote the manuscript. PBM and SMD illustrated and organized the figures. All authors have read, edited and approved submission of the manuscript.

8. References

1. Kim, S. & Wysocka, J. Deciphering the multi-scale, quantitative cis-regulatory code. *Mol. Cell* **83**, 373–392 (2023).
2. Jacob, F. & Monod, J. Genetic regulatory mechanisms in the synthesis of proteins. *J. Mol. Biol.* **3**, 318–356 (1961).
3. Davidson, E. H. *et al.* A genomic regulatory network for development. *Science* **295**, 1669–1678 (2002).
4. Mercatelli, D., Scalambra, L., Triboli, L., Ray, F. & Giorgi, F. M. Gene regulatory network inference resources: A practical overview. *Biochim. Biophys. Acta Gene Regul. Mech.* **1863**,

194430 (2020).

5. Simões-Costa, M. & Bronner, M. E. Establishing neural crest identity: a gene regulatory recipe. *Development* **142**, 242–257 (2015).
6. Claringbould, A. & Zaugg, J. B. Enhancers in disease: molecular basis and emerging treatment strategies. *Trends Mol. Med.* **27**, 1060–1073 (2021).
7. Liu, Z.-P., Wu, C., Miao, H. & Wu, H. RegNetwork: an integrated database of transcriptional and post-transcriptional regulatory networks in human and mouse. *Database* **2015**, (2015).
8. Garcia-Alonso, L., Holland, C. H., Ibrahim, M. M., Turei, D. & Saez-Rodriguez, J. Benchmark and integration of resources for the estimation of human transcription factor activities. *Genome Res.* **29**, 1363–1375 (2019).
9. Müller-Dott, S. *et al.* Expanding the coverage of regulons from high-confidence prior knowledge for accurate estimation of transcription factor activities. *Nucleic Acids Res.* **51**, 10934–10949 (2023).
10. Chen, S., Lake, B. B. & Zhang, K. High-throughput sequencing of the transcriptome and chromatin accessibility in the same cell. *Nat. Biotechnol.* **37**, 1452–1457 (2019).
11. Badia-I-Mompel, P. *et al.* Gene regulatory network inference in the era of single-cell multi-omics. *Nat. Rev. Genet.* **24**, 739–754 (2023).
12. Pratapa, A., Jalihal, A. P., Law, J. N., Bharadwaj, A. & Murali, T. M. Benchmarking algorithms for gene regulatory network inference from single-cell transcriptomic data. *Nat. Methods* **17**, 147–154 (2020).
13. McCalla, S. G. *et al.* Identifying strengths and weaknesses of methods for computational network inference from single-cell RNA-seq data. *G3 (Bethesda)* **13**, (2023).
14. Kamimoto, K. *et al.* Dissecting cell identity via network inference and in silico gene perturbation. *Nature* Preprint at https://doi.org/10.1038/s41586-022-05688-9 (2023).
15. Wang, L. *et al.* Dictys: dynamic gene regulatory network dissects developmental

continuum with single-cell multiomics. *Nat. Methods* **20**, 1368–1378 (2023).

16. Kartha, V. K. *et al.* Functional inference of gene regulation using single-cell multi-omics. *Cell Genom* **2**, (2022).
17. Kamal, A. *et al.* GRaNIE and GRaNPA: inference and evaluation of enhancer-mediated gene regulatory networks. *Mol. Syst. Biol.* e11627 (2023).
18. Fleck, J. S. *et al.* Inferring and perturbing cell fate regulomes in human brain organoids. *Nature* (2022) doi:10.1038/s41586-022-05279-8.
19. Aibar, S. *et al.* SCENIC: single-cell regulatory network inference and clustering. *Nat. Methods* **14**, 1083–1086 (2017).
20. Köster, J. & Rahmann, S. Snakemake--a scalable bioinformatics workflow engine. *Bioinformatics* **28**, 2520–2522 (2012).
21. Zhang, Z. *et al.* Single nucleus transcriptome and chromatin accessibility of postmortem human pituitaries reveal diverse stem cell regulatory mechanisms. *Cell Rep.* **38**, 110467 (2022).
22. Rich, J. M. *et al.* The impact of package selection and versioning on single-cell RNA-seq analysis. *bioRxivorg* (2024) doi:10.1101/2024.04.04.588111.
23. Harrison, P. W. *et al.* Ensembl 2024. *Nucleic Acids Res.* **52**, D891–D899 (2024).
24. Duttke, S. H., Chang, M. W., Heinz, S. & Benner, C. Identification and dynamic quantification of regulatory elements using total RNA. *Genome Res.* **29**, 1836–1846 (2019).
25. Shoyab, M., Plowman, G. D., McDonald, V. L., Bradley, J. G. & Todaro, G. J. Structure and function of human amphiregulin: a member of the epidermal growth factor family. *Science* **243**, 1074–1076 (1989).
26. Yeung, C.-M., Chan, C.-B., Leung, P.-S. & Cheng, C. H. K. Cells of the anterior pituitary. *Int. J. Biochem. Cell Biol.* **38**, 1441–1449 (2006).
27. Argelaguet, R., Cuomo, A. S. E., Stegle, O. & Marioni, J. C. Computational principles and

challenges in single-cell data integration. *Nat. Biotechnol.* **39**, 1202–1215 (2021).

28. Stuart, T., Srivastava, A., Madad, S., Lareau, C. A. & Satija, R. Single-cell chromatin state analysis with Signac. *Nat. Methods* **18**, 1333–1341 (2021).
29. Kernfeld, E., Yang, Y., Weinstock, J. S., Battle, A. & Cahan, P. A systematic comparison of computational methods for expression forecasting. *bioRxiv* (2023) doi:10.1101/2023.07.28.551039.
30. Ahlmann-Eltze, C., Huber, W. & Anders, S. Deep learning-based predictions of gene perturbation effects do not yet outperform simple linear methods. *bioRxiv* (2024) doi:10.1101/2024.09.16.613342.
31. Kernfeld, E., Keener, R., Cahan, P. & Battle, A. Transcriptome data are insufficient to control false discoveries in regulatory network inference. *Cell Syst.* **15**, 709–724.e13 (2024).
32. Yao, D. *et al.* Scalable genetic screening for regulatory circuits using compressed Perturb-seq. *Nat. Biotechnol.* **42**, 1282–1295 (2024).
33. Naqvi, S. *et al.* Precise modulation of transcription factor levels identifies features underlying dosage sensitivity. *Nat. Genet.* **55**, 841–851 (2023).
34. Labade, A. S. *et al.* Expansion in situ genome sequencing links nuclear abnormalities to hotspots of aberrant euchromatin repression. *bioRxivorg* (2024) doi:10.1101/2024.09.24.614614.
35. Avsec, Ž. *et al.* Base-resolution models of transcription-factor binding reveal soft motif syntax. *Nat. Genet.* **53**, 354–366 (2021).
36. Weber, L. M. *et al.* Essential guidelines for computational method benchmarking. *Genome Biol.* **20**, 125 (2019).
37. Zu, S. *et al.* Single-cell analysis of chromatin accessibility in the adult mouse brain. *Nature* **624**, 378–389 (2023).
38. Cusanovich, D. A. *et al.* The cis-regulatory dynamics of embryonic development at

single-cell resolution. *Nature* **555**, 538–542 (2018).

39. Zhang, K., Zemke, N. R., Armand, E. J. & Ren, B. A fast, scalable and versatile tool for analysis of single-cell omics data. *Nat. Methods* **21**, 217–227 (2024).
40. Zhang, Y. *et al.* Model-based analysis of ChIP-Seq (MACS). *Genome Biol.* **9**, R137 (2008).
41. Bredikhin, D., Kats, I. & Stegle, O. MUON: multimodal omics analysis framework. *Genome Biol.* **23**, 42 (2022).
42. Wolf, F. A., Angerer, P. & Theis, F. J. SCANPY: large-scale single-cell gene expression data analysis. *Genome Biol.* **19**, 15 (2018).
43. Korsunsky, I. *et al.* Fast, sensitive and accurate integration of single-cell data with Harmony. *Nat. Methods* **16**, 1289–1296 (2019).
44. Hao, Y. *et al.* Integrated analysis of multimodal single-cell data. *Cell* **184**, 3573–3587.e29 (2021).
45. Pliner, H. A. *et al.* Cicero predicts cis-regulatory DNA interactions from single-cell chromatin accessibility data. *Mol. Cell* **71**, 858–871.e8 (2018).
46. Heinz, S. *et al.* Simple combinations of lineage-determining transcription factors prime cis-regulatory elements required for macrophage and B cell identities. *Mol. Cell* **38**, 576–589 (2010).
47. Bruse, N. & van Heeringen, S. J. GimmeMotifs: an analysis framework for transcription factor motif analysis. (2018) doi:10.1101/474403.
48. Weirauch, M. T. *et al.* Determination and inference of eukaryotic transcription factor sequence specificity. *Cell* **158**, 1431–1443 (2014).
49. Piper, J. *et al.* Wellington: a novel method for the accurate identification of digital genomic footprints from DNase-seq data. *Nucleic Acids Res.* **41**, e201 (2013).
50. Kulakovskiy, I. V. *et al.* HOCOMOCO: towards a complete collection of transcription factor binding models for human and mouse via large-scale ChIP-Seq analysis. *Nucleic Acids Res.* **46**, D252–D259 (2018).

51. Korhonen, J. H., Palin, K., Taipale, J. & Ukkonen, E. Fast motif matching revisited: high-order PWMs, SNPs and indels. *Bioinformatics* **33**, 514–521 (2017).

52. Schep, A. N., Wu, B., Buenrostro, J. D. & Greenleaf, W. J. chromVAR: inferring transcription-factor-associated accessibility from single-cell epigenomic data. *Nat. Methods* **14**, 975–978 (2017).

53. Badia-i-Mompel, P. *et al.* decoupleR: ensemble of computational methods to infer biological activities from omics data. *Bioinformatics Advances* **2**, vbac016 (2022).

54. Ritchie, M. E. *et al.* limma powers differential expression analyses for RNA-sequencing and microarray studies. *Nucleic Acids Res.* **43**, e47 (2015).

55. Love, M. I., Huber, W. & Anders, S. Moderated estimation of fold change and dispersion for RNA-seq data with DESeq2. *Genome Biol.* **15**, 550 (2014).

56. Ambrosini, G., Groux, R. & Bucher, P. PWMScan: a fast tool for scanning entire genomes with a position-specific weight matrix. *Bioinformatics* **34**, 2483–2484 (2018).

57. Siepel, A. *et al.* Evolutionarily conserved elements in vertebrate, insect, worm, and yeast genomes. *Genome Res.* **15**, 1034–1050 (2005).

58. Castro-Mondragon, J. A. *et al.* JASPAR 2022: the 9th release of the open-access database of transcription factor binding profiles. *Nucleic Acids Res.* **50**, D165–D173 (2022).

59. McLean, C. Y. *et al.* GREAT improves functional interpretation of cis-regulatory regions. *Nat. Biotechnol.* **28**, 495–501 (2010).

60. Müller-Dott, S. *et al.* Dataset supporting the paper 'Expanding the coverage of regulons from high-confidence prior knowledge for accurate estimation of transcription factor activities'. Zenodo https://doi.org/10.5281/ZENODO.7773984 (2023).

61. Lambert, S. A. *et al.* The Human Transcription Factors. *Cell* **175**, 598–599 (2018).

62. Chari, T. & Pachter, L. The specious art of single-cell genomics. *PLoS Comput. Biol.* **19**, e1011288 (2023).

63. Feng, C. *et al.* KnockTF 2.0: a comprehensive gene expression profile database with

knockdown/knockout of transcription (co-)factors in multiple species. *Nucleic Acids Res.* **52**, D183–D193 (2024).

64. Badia-i-Mompel, P. Processed KnockTF2 experiments of human cells. Zenodo https://doi.org/10.5281/ZENODO.7035528 (2022).
65. Liberzon, A. *et al.* The Molecular Signatures Database (MSigDB) hallmark gene set collection. *Cell Syst* **1**, 417–425 (2015).
66. Kanehisa, M. & Goto, S. KEGG: kyoto encyclopedia of genes and genomes. *Nucleic Acids Res.* **28**, 27–30 (2000).
67. Milacic, M. *et al.* The reactome pathway knowledgebase 2024. *Nucleic Acids Res.* **52**, D672–D678 (2024).
68. Schubert, M. *et al.* Perturbation-response genes reveal signaling footprints in cancer gene expression. *Nat. Commun.* **9**, 20 (2018).
69. Uhlén, M. *et al.* A human protein atlas for normal and cancer tissues based on antibody proteomics. *Mol. Cell. Proteomics* **4**, 1920–1932 (2005).
70. Xu, M. *et al.* TF-Marker: a comprehensive manually curated database for transcription factors and related markers in specific cell and tissue types in human. *Nucleic Acids Res.* **50**, D402–D412 (2022).
71. Orchard, S. *et al.* The MIntAct project--IntAct as a common curation platform for 11 molecular interaction databases. *Nucleic Acids Res.* **42**, D358–63 (2014).
72. Zou, Z., Ohta, T. & Oki, S. ChIP-Atlas 3.0: a data-mining suite to explore chromosome architecture together with large-scale regulome data. *Nucleic Acids Res.* **52**, W45–W53 (2024).
73. Hammal, F., de Langen, P., Bergon, A., Lopez, F. & Ballester, B. ReMap 2022: a database of Human, Mouse, Drosophila and Arabidopsis regulatory regions from an integrative analysis of DNA-binding sequencing experiments. *Nucleic Acids Res.* **50**, D316–D325 (2022).

74. Puig, R. R., Boddie, P., Khan, A., Castro-Mondragon, J. A. & Mathelier, A. UniBind: maps of high-confidence direct TF-DNA interactions across nine species. *BMC Genomics* **22**, 482 (2021).

75. Quinlan, A. R. BEDTools: The Swiss-army tool for genome feature analysis. *Curr. Protoc. Bioinformatics* **47**, 11.12.1–34 (2014).

76. Stovner, E. B. & Sætrom, P. PyRanges: efficient comparison of genomic intervals in Python. *Bioinformatics* **36**, 918–919 (2020).

77. ENCODE Project Consortium. An integrated encyclopedia of DNA elements in the human genome. *Nature* **489**, 57–74 (2012).

78. Zhang, K. *et al.* A single-cell atlas of chromatin accessibility in the human genome. *Cell* **184**, 5985–6001.e19 (2021).

79. Sollis, E. *et al.* The NHGRI-EBI GWAS Catalog: knowledgebase and deposition resource. *Nucleic Acids Res.* **51**, D977–D985 (2023).

80. Kerimov, N. *et al.* A compendium of uniformly processed human gene expression and splicing quantitative trait loci. *Nat. Genet.* **53**, 1290–1299 (2021).

81. Virtanen, P. *et al.* SciPy 1.0: fundamental algorithms for scientific computing in Python. *Nat. Methods* **17**, 261–272 (2020).

82. Subramanian, A. *et al.* Gene set enrichment analysis: a knowledge-based approach for interpreting genome-wide expression profiles. *Proc. Natl. Acad. Sci. U. S. A.* **102**, 15545–15550 (2005).

83. Hunter, J. D. Matplotlib: A 2D Graphics Environment. *Comput. Sci. Eng.* **9**, 90–95 (2007).

84. Waskom, M. seaborn: statistical data visualization. *J. Open Source Softw.* **6**, 3021 (2021).

85. Zheng, Y., Zheng, Z., Rendeiro, A. F. & Cheung, E. Marsilea: An intuitive generalized visualization paradigm for complex datasets. *bioRxiv* (2024) doi:10.1101/2024.02.14.580236.

Supplementary Materials

Supplementary note 1

The downsampling strategy also enabled the quantification of the computational cost of running these methods (**Extended Data Fig. 2d**). Excluding the literature-derived GRNs and the random baseline, the majority of methods took less than five hours to run on 32 CPUs (full dataset mean running time = 4.24 hours), the exceptions being *Dictys* which also required a GPU, and *FigR*, which we found that its computing time grew exponentially with the number of cells and features (full dataset mean running time = 6.84 hours *Dictys*, 12.69 hours *FigR*). Regarding memory usage, most methods required more than 16 GBs (full dataset mean memory = 18.63 GBs), the exceptions being *Dictys* and *GRaNIE* (full dataset mean memory = 11.63 GBs *Dictys*, 4.6 GBs *GRaNIE*).

Extended Data Table 1. Definition of evaluation metrics. *List of evaluation metrics used to assess the performance of GRNs together with their objective and definition. Metrics that mention context-specific information were tailored for each specific dataset. For example, when working with a heart dataset only entries that contain cardiac-related labels would be used. True Positives (TP), False Positives (FP) and False Negatives (FN).*

Type	Name	Objective	Definition
Mechanistic	TF activity	Identify altered TFs in context-specific perturbation experiments	• TP = TF included in GRN with significant activity score for a perturbation experiment • FP = TF included in GRN but with insignificant activity score for a perturbation experiment • FN = TF not in GRN but in perturbation experiment
	Perturbation	Anticipate changes in gene expression after a context-specific TF perturbation simulation propagated through the GRN	• TP = TF targets included in GRN with significant Spearman correlation between predicted and observed changes in gene expression • FP = TF targets included in GRN but with insignificant Spearman correlation between predicted and observed changes in gene expression • FN = TF not in GRN but in perturbation experiment
Predictive	Omics	Independently predict omic feature readouts from other omic features from the original omics dataset. For example Gene ~ $TF_1 + ... + TF_n$. The features to use are based on the inferred GRN topology	• TP = omic feature included in GRN with significant Spearman correlation between predicted and observed molecular readouts • FP = omic feature included in GRN but with insignificant Spearman correlation between predicted and observed molecular readouts • FN = omic feature not in GRN but in omic dataset
	Gene sets	Inclusion of gene sets in GRN that are predicted to be present in the original omics dataset	• TP = gene set in GRN and omics data • FP = gene set in GRN but not in omics data • FN = gene set not in GRN but in omics data
Literature	Marker TFs	Presence of context-specific TF markers in GRN	• TP = TF in GRN and marker collection • FP = TF in GRN but not in marker collection • FN = TF not in GRN but in marker collection
	TF-TF pairs	Presence of known TF-TF interactions in GRN	• TP = TF-TF in GRN and in interactions collection • FP = TF-TF in GRN but not in interactions collection • FN = TF-TF not in GRN but in interactions collection
	TF binding	Presence of TF-CRE context-specific binding measurements in GRN	• TP = TF-CRE in GRN and in measurement collection • FP = TF-CRE in GRN but not in measurement collection • FN = TF-CRE not in GRN but in measurement collection
	CREs	Presence of annotated CREs in GRN	• TP = CRE in GRN and in annotation • FP = CRE in GRN but not in annotation • FN = CRE not in GRN but in annotation
	Regulated genes	Presence of context-specific CRE with annotated regulation to a neighboring gene in GRN	• TP = CRE-Gene in GRN and in annotation • FP = CRE-Gene in GRN but not in annotation • FN = CRE-Gene not in GRN but in annotation

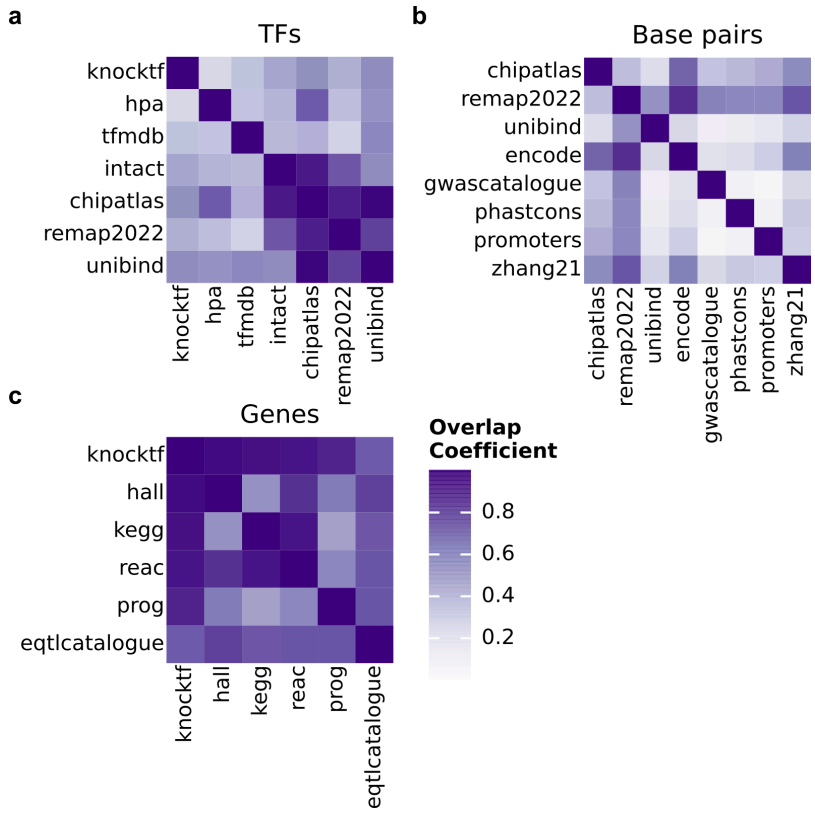

Extended Data Figure 1. Coverage across evaluation databases. *Overlap coefficient of TFs (**a**), base pairs (**b**) and target genes (**c**) across the evaluation databases.*

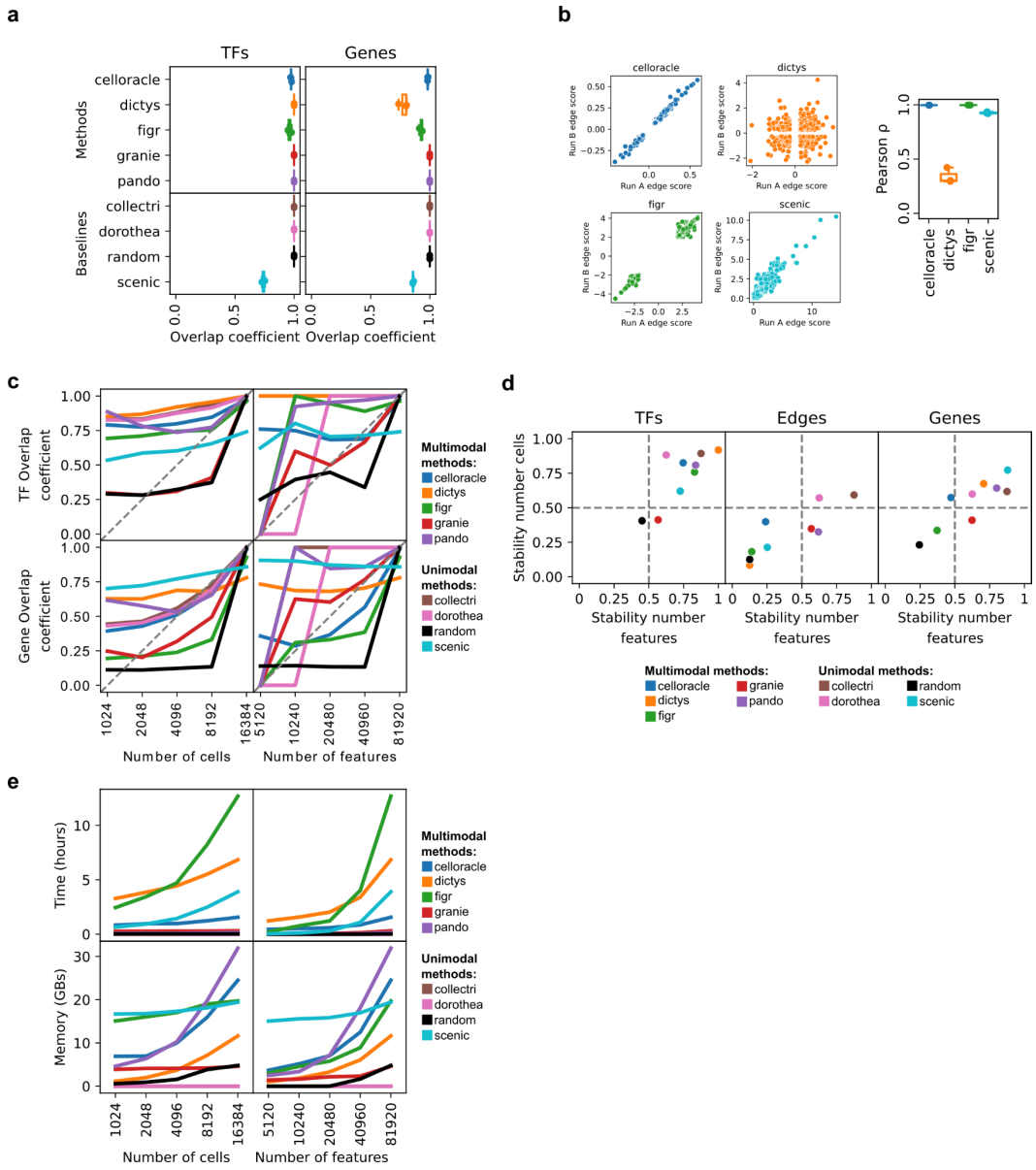

Extended Data Figure 2. ***a****, Overlap coefficients of TFs (left) and target genes (right) between three separate runs per method.* ***b****, Example comparison of edge interaction scores for the non-deterministic methods when using the same dataset (left) and thePearson ρ between the three different runs (right).* ***b****, Overlap coefficients of TFs (top) and target genes (bottom) between GRNs inferred from downsampled datasets with the one inferred using all available data.* ***c****, Stability scores for TFs, edges and target genes. The x-axis indicates the stability score when the number of cells is fixed and features are downsampled, while the y-axis indicates the stability score when the number of features are fixed and cells are downsampled.* ***e****, Mean time (top) and memory (bottom) used across methods for each downsampled dataset.*

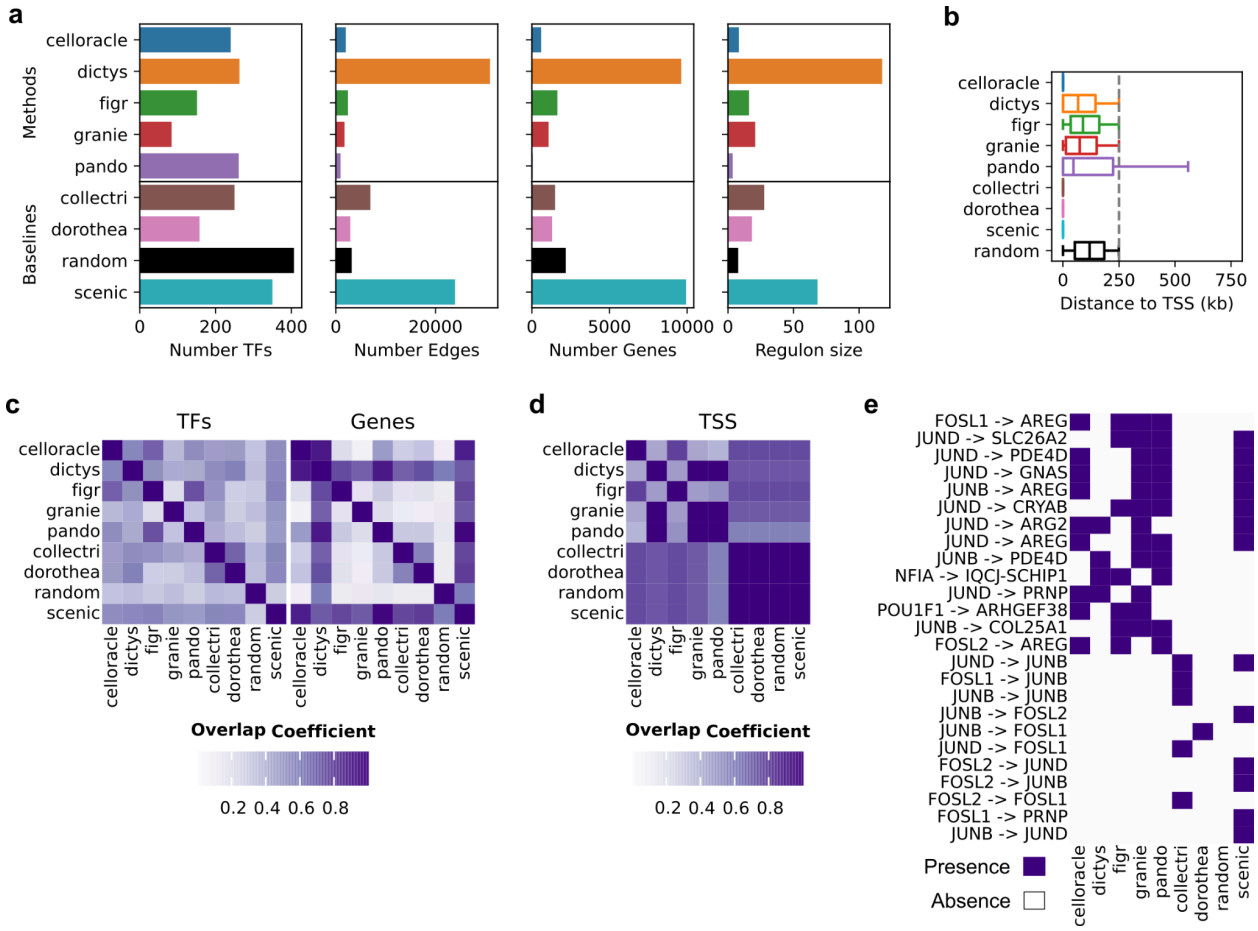

Extended Data Figure 3. ***a****, Number of transcription factors (TFs) (far left), number of edges (left), number of genes (right), and average number of target genes per TF (far right) across methods.* ***b****, Distances of Cis-regulatory elements (CRE) to transcription starting sites (TSS) by method. Dashed line indicates the window size used in all methods (± 250 kb around the TSS).* ***c****, Overlap coefficients of TFs (left) and genes (right) across methods.* ***d****, Genomic overlap coefficient of annotated TSS regions across methods.* ***e****, Binary adjacency matrix of interactions shared across at least three multimodal methods.*

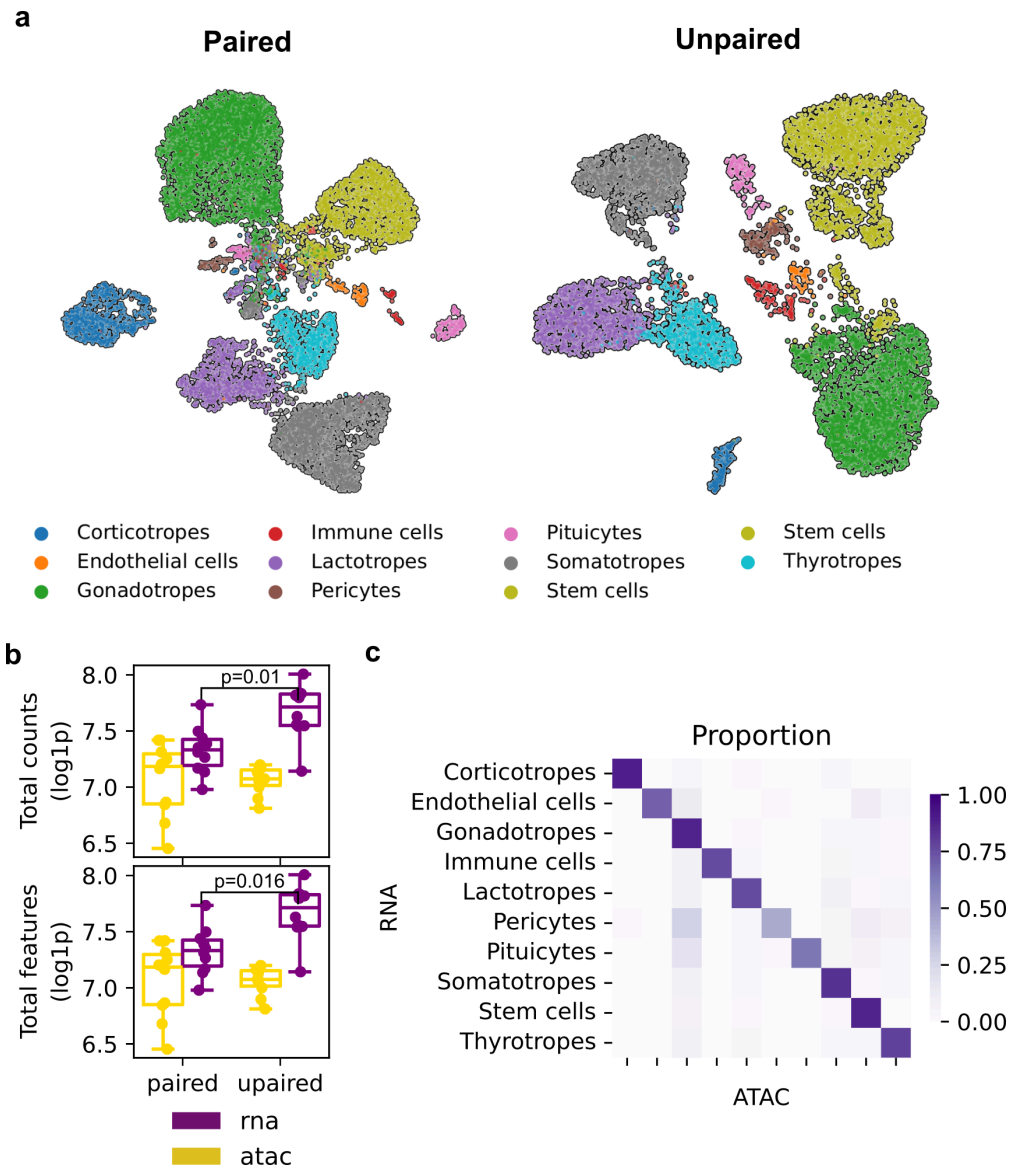

Extended Data Figure 4. Similarities between paired, unpaired and synthetic pituitary datasets. a, *UMAP visualization of the cell type clusters for the paired (left) and unpaired (right) datasets. Color represents the different cell types.* ***b****, Mean total number of counts and mean number of features with counts per cell type for the paired and unpaired dataset.* ***c,*** *Proportion of barcodes from one cell type matched to the others after integration in the synthetic paired dataset.*

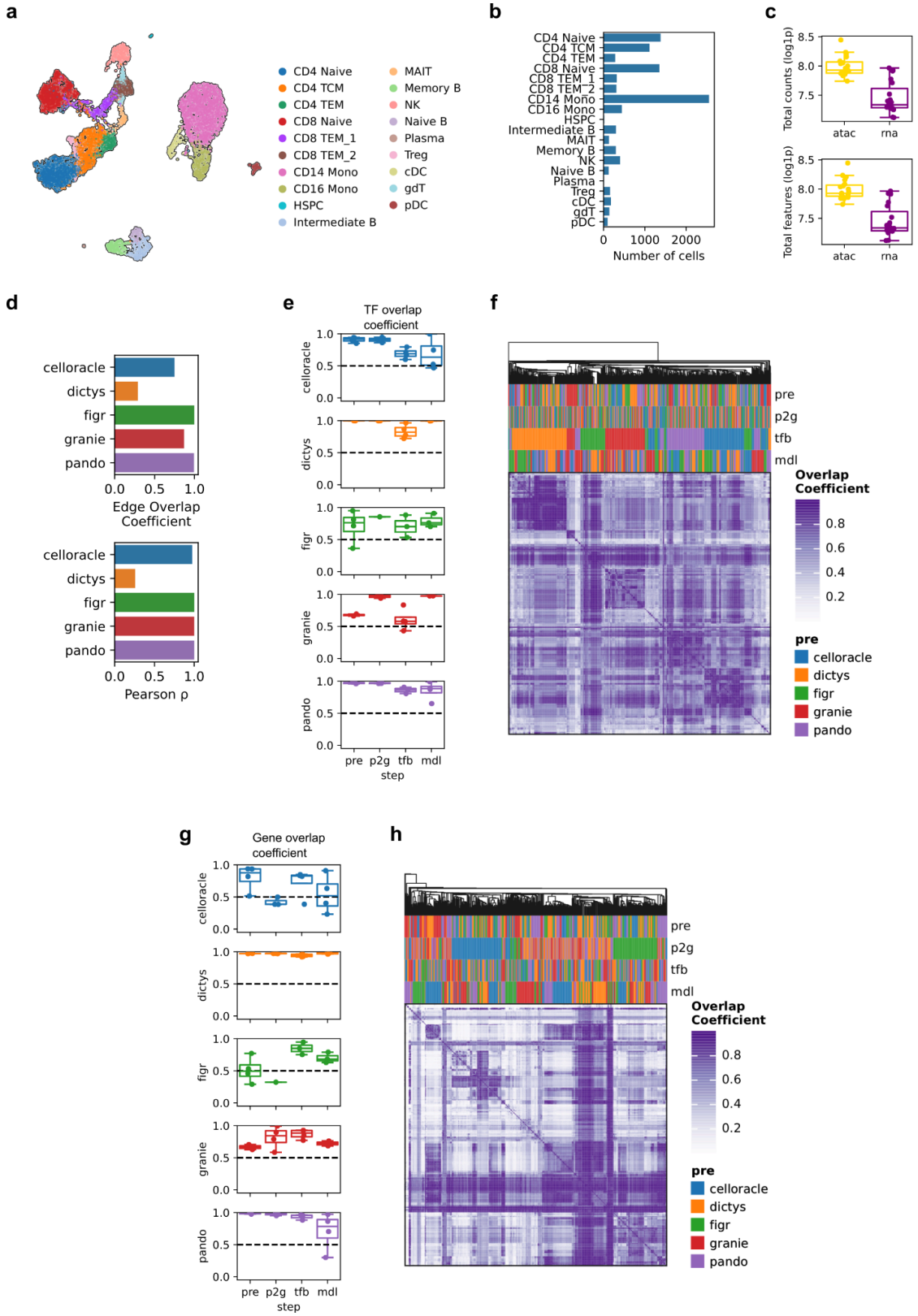
a
CD4 Naive
CD4 TCM
CD4 TEM
CD8 Naive
CD8 TEM_1
CD8 TEM_2
CD14 Mono
CD16 Mono
HSPC
Intermediate B
MAIT
Memory B
NK
Naive B
Plasma
Treg
cDC
gdT
pDC
b
Number of cells
c
Total counts (log1p)
Total features (log1p)
atac
rna
d
celloracle
dictys
figr
granie
pando
Edge Overlap Coefficient
Pearson ρ
e
TF overlap coefficient
pre
p2g
tfb
mdl
step
f
Overlap Coefficient
g
Gene overlap coefficient
h

Extended Data Figure 5. Peripheral blood mononuclear cell dataset and similarities between runs. a, *UMAP visualization of the cell type clusters for the peripheral blood mononuclear cell dataset. Color represents the different cell types.* ***b****, Number of cells per cell type.* ***c****, Mean total number of counts and mean number of features with counts per cell type.* ***d****, Overlap coefficient at the edge level (top) and Spearman's* ρ *(bottom) between the original methods and their equivalent decoupled counterpart (top).* ***e****, Effect of changing one of the inference steps from a fixed method pipeline to another method, measured by the overlap coefficient at the TF level.* ***f****, Pairwise overlap coefficient at the TF level between all possible inference runs combinations.* ***g****,* ***h*** *are the same as* ***e*** *and* ***f*** *but for the overlap coefficient at the gene level.*

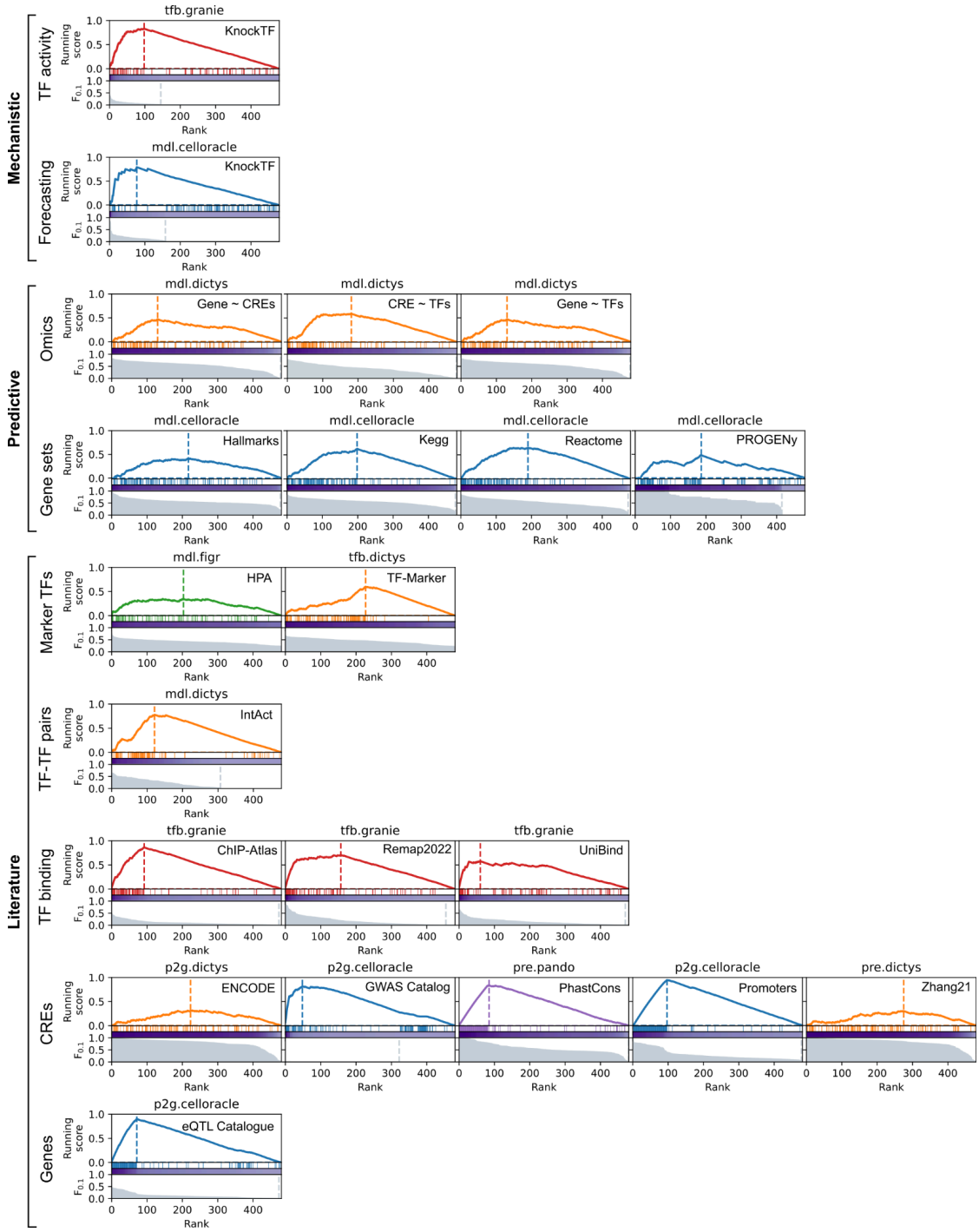

Extended Data Figure 6. Weighted Kolmogorov-Smirnov-like statistics plots. *Weighted Kolmogorov-Smirnov-like statistic plots of the inference step method combination with the most significant p-value for each evaluation task.*

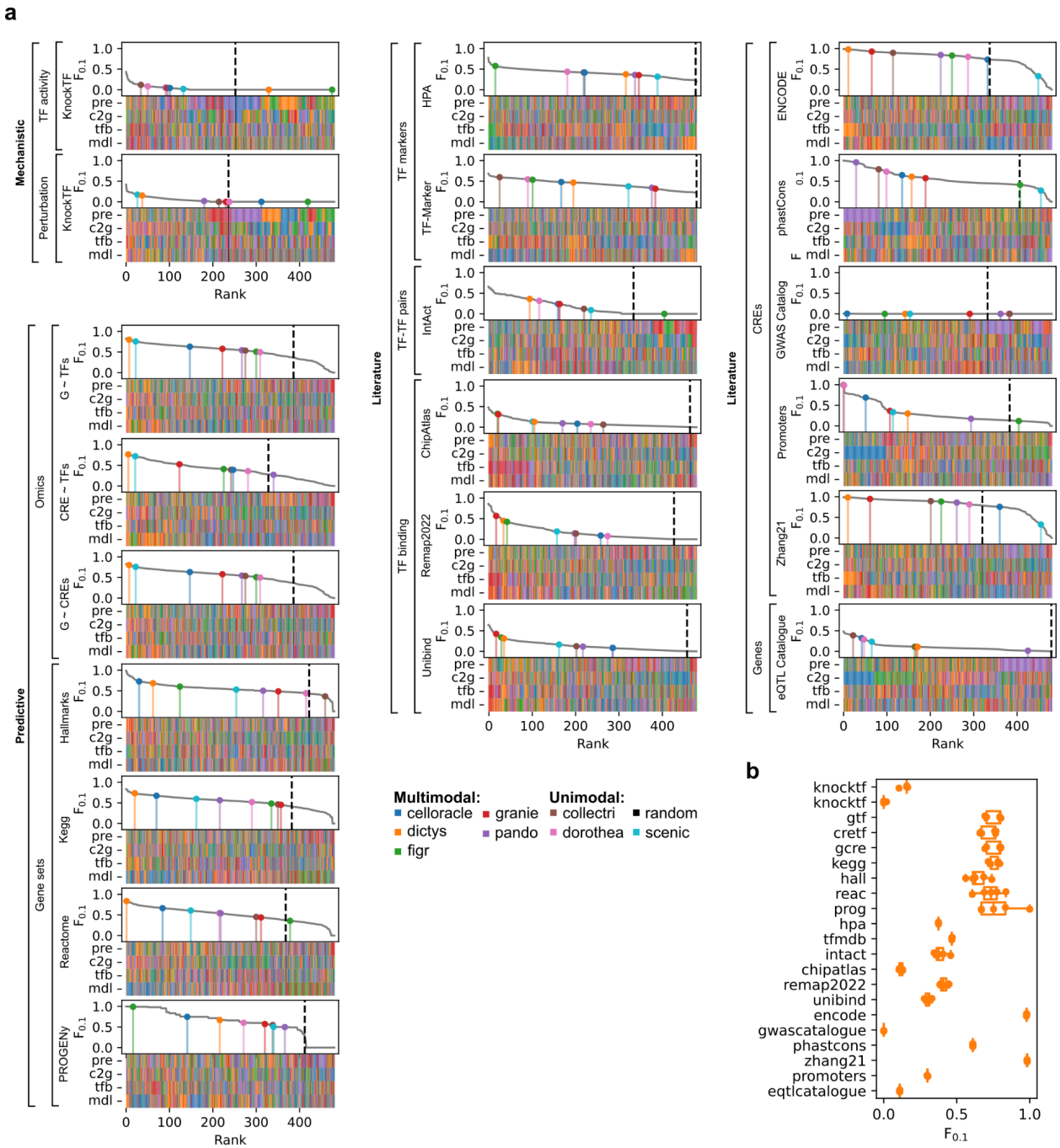

Extended Data Figure 7. Performance of fixed multimodal and unimodal methods. a, *Ranks of fixed multimodal and unimodal methods across evaluation tasks.* ***b****, Stability of performances for fixed Dictys runs using five different random seeds.*